university of groningen / faculty of science and engineering

SRON Netherlands Institute for Space Research

Bachelors Thesis in Applied Physics

PERFORMANCE ANALYSIS OF LOW TEMPERATURE SUPERCONDUCTING FLUX PUMP

Researched at SRON Groningen, the Netherlands

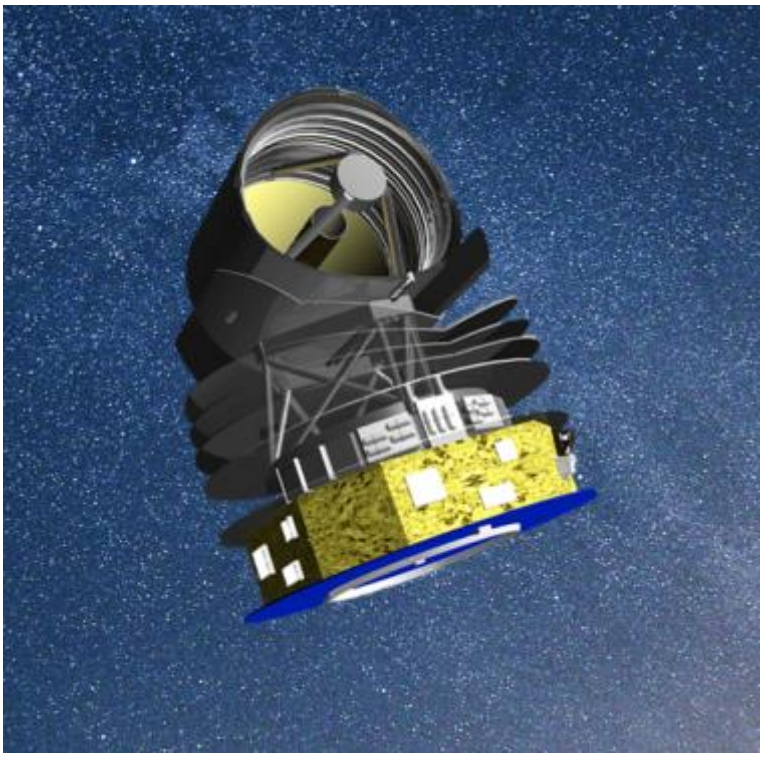

July, 2017

James Robert Lyon, S2709821
j.r.lyon@student.rug.nl / (+31)619671537
Faculty of Science and Engineering
University of Groningen

Supervised by
dr. ir. G. de Lange (SRON)
prof. dr. ir. C.H. van der Wal (RUG)
prof. dr. T. Banerjee (RUG)

[This page intentionally left blank]

Abstract

A flux pump system uses a small alternating current to build up a large current inside a superconducting load coil. An experimental prototype has been built for the purpose of analysing its performance, including its stability, reliability and limiting, for possible satellite application at SRON. The flux pump circuit is a developing project previously worked upon by two other Bachelor students.

The operation of the full wave transformer rectifier flux pump is described and analysed. The experimental set-up was rebuilt, measurement methods were developed and sensors were calibrated. The optimal primary wave for this device was experimentally determined to have a frequency of 0.1667 Hz and amplitude of 250 mA from which an exponential increase was observed and a maximum output of approximately 7 A was achieved. However, it proved to be an unreliable system as repeated experiments provided inconsistent results due to suspected short circuiting of inductors. Moreover, the power and efficiency of the system is analysed and is in good agreement with theoretical predications. The flux pump has a maximum efficiency of 80% at a normalised current of 0.2.

Contents

Acknowledgments

Throughout my time working on this Bachelors Project, there a group of people I wish to thank for their help, advice and support. Without whom I would not have developed or learnt the skills which enabled me to compile this report.

They are:

- **Gert de Lange** – Gert was my supervisor at SRON whose expert knowledge and understanding was critical in my research. Patient, encouraging and wise; I greatly appreciate his help and support.

- **Willem-Jan Vreeling** – Willem's wealth of knowledge in all things technical helped me understand essential measurement equipment and probably saved me from blowing something up. His willingness to help and patience are much appreciated.

- **Laurens Even** – Laurens is a Masters student in Physics at RuG who worked on this flux pump project for his Bachelors thesis in 2016. He continuously supported me via WhatsApp answering any questions I had and even visited me a couple of times in the laboratory to help.

- **Duc van Nguyen and Henk Odé –** Duc for his help and advice with electrical related questions and Henk for his steady hand in soldering delicate components of the circuit.

- **Jarno Panman and Rob van der Schuur -** For their help and advice with mechanical related questions. Specifically, showing me how to use the equipment in the workshop.

- **Bert Kramer –** For his help in cooling the cryostat.

- **Heino Smit –** For his help in understanding the operation of the hall sensor.

- **Prof. van der Wal and Prof. Banerjee** – For agreeing to be my supervisors from the University and taking on another report to mark - I only wish them an enjoyable read.

[This page intentionally left blank]

Layout of this Report

The layout of this report has been tailored to increase readability. Following this section, chapter 1 provides background information regarding the research as well as specifying the aims of this report. Further on, some information about SRON and the origin of this research is presented.

In chapter 2, relevant theory from studied literature is derived and stated. Starting from fundamental physics such as solid state and electrodynamics, the theoretical operation of a flux pump circuit is built up.

Chapter 3 contains all information regarding the experimental set up. Here, you can find information about how the flux pump circuit was built, the operation of the cryostat, the data processing units, power supplies and the LabVIEW program used to measure and operate the system.

The main body of this report is chapter 4 which documents the experimental results and analysis. It is divided into six chronological sub-sections.

Chapter 5 concludes the report. This provides an overview of the important experimental results obtained as well as commenting on various other aspects - such as the validity of theoretical equations or the reliability of the measuring methods used. Most importantly, it will return to and answer the success of the research aims.

Presented at the end of the report is a bibliography and appendices for the reader's discretion.

1 Introduction

1.1 Background Information

A flux pump circuit is an eloquent electrical circuit that operates at superconducting temperatures. A useful analogy one could use to understand the principle of a flux pump would be to compare it to a balloon. Using breaths of air; one can store a large volume of air inside a latex balloon. A flux pump circuit uses a small alternating current to build up a large current inside a superconducting load coil.

The advantages of using a flux pump circuit for applications of superconducting technology that use large currents (~1 kA) are well known [1]. Consider a superconducting magnet that uses a direct power supply; when delivering these currents to a low temperatures environment region Joule heating can cause undesirable effects. For example, the power produced by 1000 A in a copper wire of 1 m in length with a cross-sectional area of 1 cm^2, assuming a uniform temperature gradient between 300 K and 4.2 K, is over 150 W. Large current supplies require thick wires which in turn produce a bigger parasitic heat load. Long-term operation of a high-current superconducting magnets using room temperatures power supplies is costly in terms of liquid helium boil off. For laboratory uses these losses can sometimes be acceptable, for technical and commercial operation, reduction of these losses is desirable [2]. In those cases where the current build-up in a superconducting coil does not have to be very fast, a flux pump can be used to overcome the mentioned problems. By using small cumulative current increments to a load coil, you can charge a superconducting coil whilst improving the Joule heating .

For the past two years, SRON (the Netherlands Institute for Space Research) has enrolled the help of Bachelor students to research and develop a flux pump system for satellite application. Wim van den Berg from the Saxion University of Applied Science was the first student to work on this project, succeeded by Laurens Even from the University of Groningen. Van den Berg is responsible for the initial research and design of the circuit analyzed in this report [3]. Despite his best efforts, van den Berg did not observe flux pumping in the circuit he built. It wasn't until Even noticed flaws in the original circuit design and was able to observe the circuit in operation [4]. Unfortunately, due to time constraints, Evens wasn't able to characterize and analyses the circuit. Thus, it is with great pleasure that, within this report, I shall present the continued work that I have carried out on the flux pump system.

1.2 Research Aims

The main goal of this research paper is to analyses the performance of the mentioned flux pumping system including its stability, reliability and limiting current being measured.

Aim 1: Improve the sensing element for measuring the load coil current

Although Even observed an increasing magnetic field when the flux pump was in operation, the range of magnetic field sensor meant only a maximum current of approximately 60 mA could be detected in the load coil. Considering the fact that a peak primary current of 250 mA was being used, only being able to detect an output current that is four times smaller than the input isn't any good for characterizing the system and defeats the purpose of a flux pump. Therefore, an aim of this report is install a better sensor for measuring larger load coil currents.

Aim 2: Determine the optimal primary wave for charging

The maximum current that the superconducting load coil can store depends on the peak primary current and the charging rate depends on the frequency of the primary wave. Although it may be logical to use very large values, one must consider factors such as Joule heating, thermal switching, reliability and efficiency. Ultimately, the primary wave used will be decided as a tradeoff between several of these factors. Thus, it is in the interests of characterizing the flux pump to determine this optimal wave.

Aim 3: Measuring the load coil current until saturation

The main characteristic of this flux pump will be the increasing exponential load coil current as a function of time. Therefore, after research aims 1 and 2 have been realized, several experiments will be executed in order to "pump" the circuit to saturation. From this information, characteristics such as the limiting current value and the reliability of the system can be determined.

Aim 4: Perform a power and efficiency analysis on the flux pump circuit

As mentioned, the origin of the research stemmed from using a flux pump circuit for possible satellite application. Therefore, performance characteristics like efficiency and power used will be analyzed.

1.3 About SRON

The Netherlands Institute for Space Research, abbreviated to SRON, is the Dutch answer to NASA. Established in 1983, the institute strives to be at the forefront in the development of state-of-the-art satellite instruments for international space research. Quality driven and pioneering, the technology of SRON has contributed to multiple ground-breaking missions [5].

FIG 1.1 An SRON employee working HIFI, one of the three scientific instruments of Herschel.

1.4 Why SRON are interested in flux pump system

The research conducted in this report is inspired and driven by the SPICA/SAFARI mission. Originally, the proposed measuring element was a Fourier Transform Spectrometer (FTS). The FTS includes a movable mirror which is suspended in magnetic bearing with a magnetic linear stage providing the ability for the mirror to move. To test this system on Earth, the magnetic bearings must provide a magnetic field strong enough to compensate the effects of gravity - this is called '1G-off-loading'. It is in the of the SPICA/ SAFARI mission that any parasitic heat load must be minimized; hence SRON taking an interest in the principle of a flux pump to power a superconducting coil to produce the said magnetic fields.

It uncertain if a flux pump will be used for the FTS as changes have been made to the original design. None-the-less, the application of a flux pump for energy storage, high current test beds and levitation, is still in the interest of SRON.

1.5 About the SPICA/ SAFARI Mission

The purpose of this mission is to launch a Japanese built satellite named SPICA (Space Infrared Telescope for Cosmology and Astrophysics) that will have the ability to look deeper into space than the current Herschel telescope[1]. SAFARI is the European 'nerve centre' of the space telescope, and is being developed under the leadership of SRON.

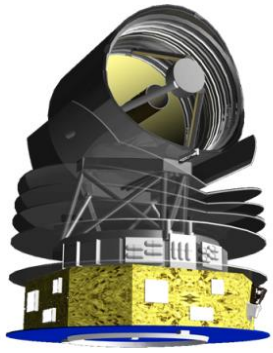

FIG 1.2 The SPICA satellite, to be launched in 2028.

SAFARI is an infrared spectrometer that will be able to fully utilize the sensitivity of the extremely cool (approximately < 1 K) Japanese designed mirror [6]. The extremely low operating temperatures allow the detectors to no longer be 'bounded' by the thermal radiation coming from the mirrors

[1] The Herschel Space Observatory was a space observatory built and operated by the European Space Agency (ESA). It was active from 2009 to 2013, and was the largest infrared telescope ever launched, carrying a single 3.5-metre mirror and instruments sensitive to the far infrared and submillimeter wavebands (55–672 μm). [20]

itself, thus enabling the ability to detect orders of magnitude two times weaker than Herschel. This impressive instalment in the next chapter of research detection capabilities can not only search in the far infrared waves of the first galaxies, but also for ice and water vapour in protoplanetary discs.

The expected launch year is 2028.

2 Theoretical Background

A flux pump systems applies relatively fundamental physics, such as electronics, electricity and magnetism and solid state physics, in an ingenious manner.

2.1 General Physics Concepts

Some well-known physical concepts will be briefly discussed before moving onto the step-by-step operation of a flux pump circuit.

2.1.1 Superconductivity

Superconductivity is a physical phenomenon where certain materials, superconductors, exhibit exactly zero electrical resistance below a certain critical temperature. Thus, an induced current in a superconducting ring can be sustained for a very long time without any measureable reduction. Furthermore, another property of superconductors is that they will completely eject magnetic fields lines from its interior as it transmissions to its superconducting state.

Superconductivity is a quantum mechanical wonder which can be explained by the BCS theory[2]. In short, the theory describes that materials suddenly become extreme conductors when the electrons inside them join forces to make what are call Cooper pairs. In regular materials, the current carrying electrons are scattered by various defects and vibrations with inside the crystals structure - these imperfections are the cause for electrical resistance. Compared to cooled superconductors, the Coopers paired electrons can move more freely without being scattered [7].

2.1.2 Mutual Inductance of a Coil Wrapped Around a Solenoid

Suppose that there are two loops of wire at rest (Fig. 2.1). It is well known in electrodynamics that, if a steady current I_1 were to pass around loop 1, that it would produce a magnetic field B_1 [8]. Some of the field lines would pass through loop 2; let Φ_2 be the flux of B_1 through 2.

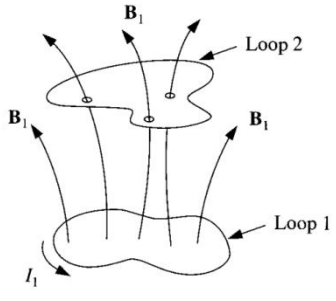

FIG 2.1 Two loops of wire, at rest.

[2] Bardeen-Cooper-Schrieffer theory name after John Bardeen, Leon Cooper and John Robert Schrieffer.

From Biot-Savart law, the magnetic field B_1 is directly proportional to the current I_1. Therefore, so too is the flux through loop 2

$$\Phi_2 = MI_1,$$

where M is the constant of proportionality, known as the mutual inductance of the two loops. It is a purely geometrical quantity, having to do with the sizes, shape, number of turns and relative positions of the two loops.

Consider now if the current in loop 1 was to vary with time. The flux in loop 2 will vary accordingly, and Faraday's law dictates that this changing flux will induce an emf (electric motive force) ε_2 in loop 2,

$$\varepsilon_2 = -\frac{d\Phi_2}{dt} = -M\frac{dI_1}{dt}. \quad (1)$$

This means that every time the current though loop 1 change, an induced current will flow through loop 2 – even though there is no physical connection.

An emf ε_1 will also be induced in loop 1

$$\varepsilon_1 = -L\frac{dI_1}{dt}, \quad (2)$$

where L is called the self-inductance of the loop and, like M, depends solely on geometry. Inductance is measured in Henries H; a Henry is defined as a volt-second per ampere.

2.1.3 Superconducting Magnets

A superconducting magnet is an electromagnet made from the coils of a superconducting wire which must be cooled to cryogenic temperatures during operation [9]. When in its superconducting state, the wires can withstand much larger electric currents than ordinary wires creating very strong magnetic fields which can be used in MRI machines, particle accelerators and other scientific applications.

However, many disadvantages and problems can occur when delivering these currents to a low temperature.

When a superconducting magnet is in its steady state, the only voltage across the magnet is due to the resistance of the wires that connect the power supply to the superconducting coil. Thus, the power to the coil windings is provided by a high current, low voltage DC power supply. Any change in to the current must be done very slowly in order to avoid a large voltage spike across the windings of the coil - as essentially the magnet is a very large inductor. Furthermore, fast changes in current will cause mechanical stresses in the windings or eddy currents that will encourage the magnet to quench.

The energy E that can be stored in a superconducting magnet is described by

$$E = \frac{1}{2}LI^2 . \quad (3)$$

2.1.4 Magnetic Quenching

Magnetic quenching can be a rather dramatic and dangerous event that can occur in superconducting magnetics. It occurs when superconducting magnets warms above a critical temperature. Parts of the superconducting wire in the magnet lose their ability to conduct electricity without resistance, generating more heat that quickly engulfs the whole magnet and causing the coolant surrounding the magnet to boil [10]. In large superconducting magnets carrying thousands of amperes, such a quench could generate the force of an exploding stick of dynamite.

2.2 Flux Pump

The basic operation of a flux pump circuit is its ability to build up and maintain large currents at cryogenic temperatures being only supplied by an acceptably low power supply. The underlying principle of the system is the transfer of flux.

A large number of flux pumps have been proposed and built. Although they operate in completely different ways, the all show the essential 'pumping' behaviour of electrical current [2]. One example is a flux compressor; which is mechanically operated and traps magnetic fields inside a superconducting cylinder. Another example is the superconducting DC dynamos, which turn mechanical energy into electromechanical energy. Finally there are transformer rectifier flux pumps, which are similar to electrical transformers.

The full name for the flux pump circuit investigated in this report is the "Full Wave Transformer Rectifier Flux Pump". This circuit is generally regarded as the most promising flux pump design.

2.2.1 Full Wave Transformer Rectifier Flux Pump

Shown below is a schematic drawing of the full wave transformer rectifier flux pump (Fig. 2.2).

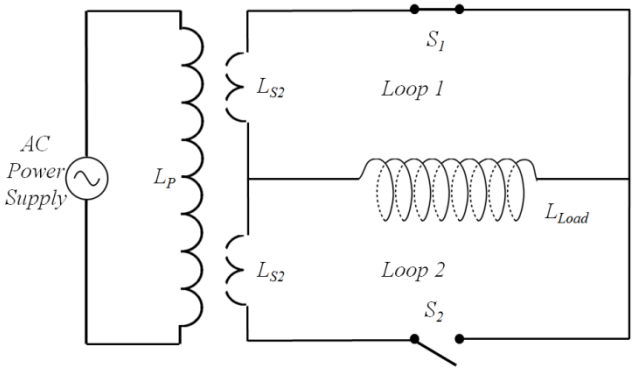

FIG 2.2 Full wave rectifier flux pump.

There are four superconducting inductors, three of which are incorporated into a centre-tapped transformer, with primary inductance L_P and secondary inductance L_{S1} and L_{S2}. The coupling between the secondary coils is denoted as k_{12}, and the coupling between the primary and the secondary coils is k_{PS}. The forth superconducting inductor is the load coil and is responsible for generating the high magnetic fields. The load coil has inductance L_L and is assumed to have no mutual inductance with the transformer. Current is transferred between the two loops by operation the two switches S_1 and S_2 [1].

The operation of the flux pump can be divided into 4 steps (Fig. 2.3).

Step 1

Initially, there is no current flowing anywhere in the flux pump circuit. Switch 1 is closed and switch 2 is open – thus no current can be induced in loop 2. The primary current increases to its maximum amplitude I_P. As mentioned in section 2.1.2, this will induce a current i_1 in loop 1 which will, according equation (4), be equal to

$$i_1 = -2I_p \frac{M_{PS}}{L_S + L_L} \qquad (4)$$

where $2L_S = L_{S1} + L_{S2}$ and $M_{PS} = k_{PS}\sqrt{L_P L_S}$.

The negative sign indicated that his current is opposing the flux in L_1 produced by the primary coil.

Step 2

While the primary current remains constant, switch 2 is closed.

Step 3

While the primary current remains constant, switch 1 is now open. This cause a decay of the current in loop 1, resulting in a back emf across L_L producing a current i_2 in loop 2, which by conservation of flux is given by

$$i_2 = i_1 \frac{L_L - k_{12}L_S}{L_L + L_S} \qquad (5)$$

For the sake of clarity, a new symbol is defined as $\alpha = \frac{(L_L - k_{12}L_S)}{L_L + L_S}$

Step 4

The primary current decreases to its minimum amplitude $-I_P$ willproduce a current increment in loop 2, again in order to conserve flux, which has the same magnitude as i_1. Thus the total current in loop 2 is

$$i_3 = i_2 + 2I_p \frac{M_{PS}}{L_S + L_L}. \qquad (6)$$

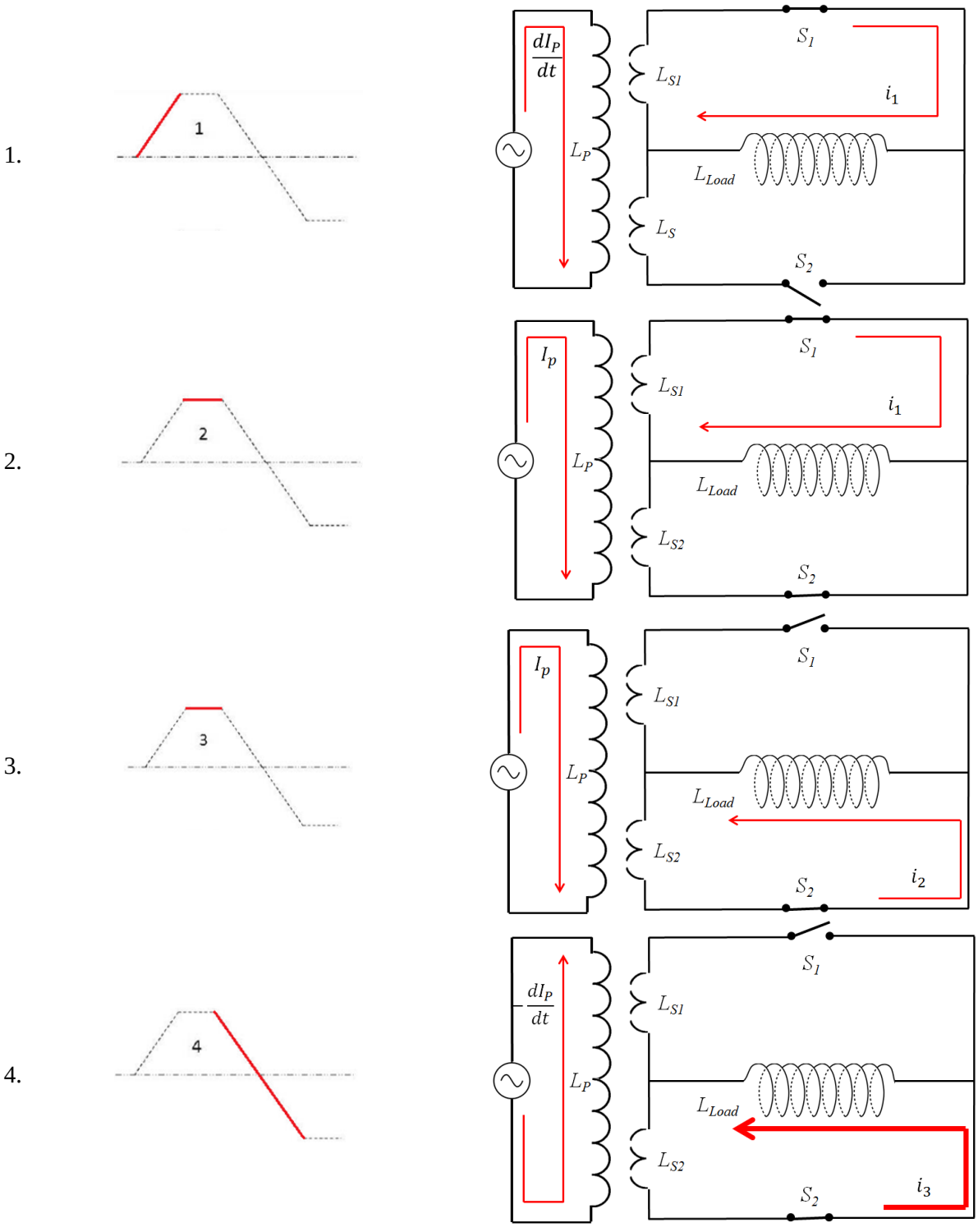

FIG 2.3 The primary and seconday circuit currents during operation of a transformer-rectifier flux pump in resistive transfer.

Opening switch 2 and closing switch 1 transfers the fraction α to current in loop 2 into loop 1 [1]. Now the flux pump has completed one cycle and is now in its original configuration, except that there is a current

$$I_L^{(1)} = i_1(\alpha + \alpha^2) \tag{7}$$

in the load coil. After n cycles, the current in the load coil is

$$I_L^{(n)} = i_1(\alpha + \alpha^2 + \cdots + \alpha^{2n}). \tag{8}$$

From equation (7) and equation (8) the maximum load current obtainable is

$$I_L^{(\max)} = 2I_P k_{PS} \sqrt{\frac{L_P}{L_S}} \cdot \left(\frac{\alpha}{k_{12} + 1}\right) \tag{9}$$

For the majority of flux pumps, $L_L \gg L_S$. For this case of a large primary/secondary ratio and assuming that $k_{12} = 0$, it can be shown quite easily that equation (9) reduces to

$$I_L^{(\max)} = 2I_P k_{PS} \sqrt{\frac{L_P}{L_S}}. \tag{10}$$

Finally, the characteristics number of cycles n_0 can be approximated by

$$n_0 \approx \frac{L_L}{2L_S}. \tag{11}$$

Equation (10) and equation (11) can characterize any flux pump driven by any load. There is clearly a trade-off between the rate of rise of load current (determined by the ratio L_S/L_L) and the maximum current attainable (determined by $\left(\frac{L_P}{L_S}\right)^{\frac{1}{2}}$).

2.2.2 A Different Perspective Using Circuit Analysis

Using figure 2.2 and applying conventional circuit analysis, one can determine the load current, I_L, and average load charging voltage, u_L, for resistive transfer operation. The voltage across the load coil within a given pumping half-cycle is given by

$$u_L(t) = \frac{1}{2}[2I_P \pi f M_{PS} \sin(2\pi f t) - I_L R \exp\left(-\frac{Rt}{2L_S}\right)] \tag{12}$$

where $u_L$is the instantaneous voltage, R is the open state resistance of the switches and I_L is the load current at $t = 0$. The negative term in equation (12) is an exponentially decaying voltage spoke impressed across the load during gate switching.

Using equation (12) as a starting point, one can derive a function for the load coil current as a function of time

$$I_L(t) = 2I_P k_{PS} \sqrt{\frac{L_P}{L_S}} \left[1 - \exp\left(\frac{f L_S}{2L_L}\, t\right)\right]. \quad (13)$$

we note that load current rise exponentially to a limiting value given by

$$I_L(\infty) = 2I_P k_{PS} \sqrt{\frac{L_P}{L_S}} \quad (14)$$

which is identical to the expression for maximum load current developed using the flux conservation.

2.2.3 The Rise and Fall of Power

It is well known that electrical power is given by

$$P = IV\,. \quad (15)$$

Power input to the load coil, P_L, is given by

$$P_L = I_L \times L_L \frac{dI_L}{dt}\,, \quad (16)$$

which, from equation (12) gives

$$P_L = f\left(2M_{PS} I_P I_L - 2L_S {I_L}^2\right). \quad (17)$$

In terms of normalized load current $\left(n = I_L / I_L^{(\max)}\right)$,

$$P_L = (n - n^2) f \frac{(2M_{PS} I_P)^2}{2L_S}\,. \quad (18)$$

Considering flux pump losses are solely due to the resistive dissipation in the normal loop state, several authors give the expression ([1] [2] [11] [12] [13] [14]) for total thermal switch loss as

$$P_{Loss} = 2fL_S{I_L}^2 + \frac{(2\pi f M_{PS} I_P)^2}{R}, \qquad (19)$$

where R is the resistance of either loop 1 or 2 in its resistive state.

2.2.4 The Difference Between Inductive and Resistive Operation

There are two possible steps in which the manner of the load current is commutated between the gates at each half-cycle (ie. before the switches change) – inductive transfer and resistive transfer [15]. The problem with the resistive method is that is suffers due to resistive dissipation in the normal state gate during load current transfer - energy in the loop proportional to I_L^2 will be dissipated.

In inductive transfer mode, at the end of the pumping period the primary current is constant for a moment while the second switch closes so that both secondary loops are superconducting. Using a suitable step in the primary current δI_P, which will in turn, induce a circular current I_S in the now short circuited secondary circuit. If the magnitude of the primary current step is chosen to make $I_S = I_L$, then the current in switch S_1 is cancelled. Then the primary current remains constant for a moment and allows the 'current-zero' to be opened without any losses.

Simply by judging the length of their respective explanations, it is obvious that resistive transfer operation is a far simpler method as it does not require electronic controls logic and programmable power supplies. However it has been tested [15], that in its simplicity lies substantial energy losses and reductions in efficiency.

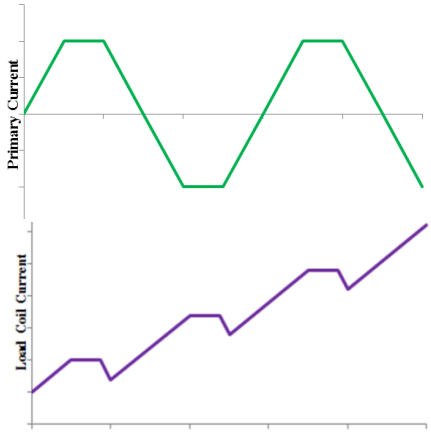

FIG 2.4.a The top graph shows the wave form used in resistive transfer. The bottom graph shows the load coil current increase with small decreasing dips that are because of the energy dissipated.

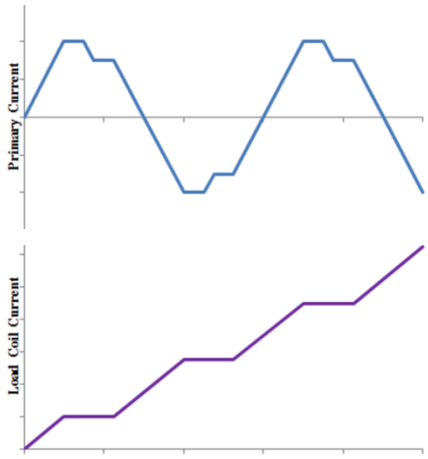

FIG 2.4.b The top graph shows the wave form used in inductive transfer with step of magnitude δI_P which reduces in losses in the load coil current as can be seen in the bottom graph.

3 Experimental Set-up

3.1 General Description

The experimental set-up consists of a flux pump circuit placed inside a cryostat which will be cooled down to cryogenic temperatures. Various break boxes, data acquisition units and power supplies are set up outside the cryostat chamber to measure and process data and supply power to the various components of the internal flux pump circuit. The data is connected to a computer in which the system engineering software 'LabVIEW 2014' can manage the data. LabVIEW is also used to program, control and monitor the several of parameters of the LabVIEW circuit – for example, you can control the primary wave signal.

For clarification purposes, the set-up can essentially be divided into three sections

1. Inside the cryostat chamber – this includes the actual flux pump circuit itself.
2. Outside the cryostat chamber – including powers supplies, break boxes and data accusation units.
3. Digital interface – in other words, the LabVIEW program.

3.1.1 Disclaimer

The experimental set-up described is largely based upon the impressive and hardworking students who I have succeeded in this research. Credit where credit is due, Wim van den Berg and Laurens Even in their reports provided valuable information and comment on the set-up of the flux pump experiment.

Van den Berg is responsible for original flux pump design used in this experiment. There are multiple proven ways to simulate the flux pump principle; it was van den Berg who chose to build and investigate the full-wave rectifier design. He also designed the hexagon shaped primary coil to minimize stray magnetic fields. Van den Berg is also the architect of the impressive and complex LabVIEW program used to run this experiment.

Laurens Even continued the research of van den Berg and is responsible for making the flux pump circuit work. He made several changes to van den Berg's design, including the redesign of the primary coil to increase its self-inductance and the correction of the winding orientation of a secondary coil in the transformer.

The design choices and tweaks made by van den Berg and Even will be commented on further in the following sections of this report. For the sake of clarity and continuity purposes from previous report, the experimental set-up used by van den Berg will continue to be called V2.0 and Even's setup will be V3.0. To keep with this trend, the changes that I have made will be noted as V4.0.

3.2 Inside the Cryostat Chamber

The inside of the cryostat chamber is home to the flux pump circuit itself.

3.2.1 Flux Pump Circuit V3.0

Shown below in figure 3.1 is a schematic of the flux pump circuit V3.0. Everything inside the dashed green box represents the various components that are found inside the cryostat chamber. It should be noted that the temperature sensor, fluxgate and extra secondary coil are not essential components of a flux pump circuit and are purely used for measurement purposes only.

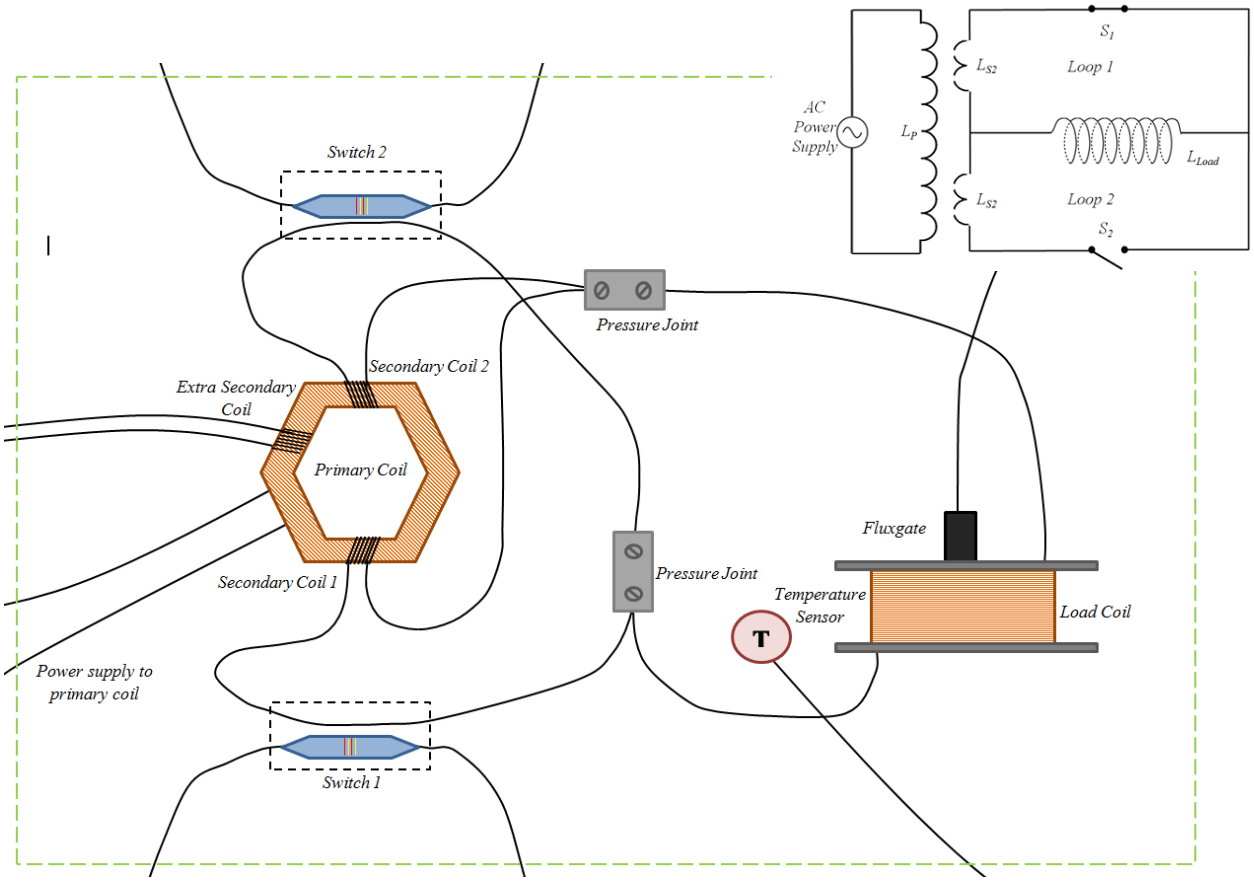

FIG 3.1 Schematic drawing of the flux pump circuit V3.0. Shown in the top right corner is figure 2.2 for comparison purposes. Please see figure 3.4 for an actual picture of the flux pump circuit.

Shown on page 22:

The Primary Coil The primary coil is hexagonal in shape having been made up of 6 straight coils fitted together at 30º. The core is made of Vespel polyamide [3] with 70 μm Niomax-CN A61/05 wiring wrapped around 4950 turns. The room temperature resistance of the coil is 17.45 kΩ with a measured self-inductance of 4.449 mH. The coil is encapsulated in a thermally conductive epoxy which improves the thermal contact with the copper ground plate.

The Secondary Coils The secondary coils have a total self-inductance of 0.58 μH as calculated using "Multi-Layer Coil Inductance Calculator". taking the inner diameter of 5.4 mm, length of 10 mm and for 10 turns and multiplying by 2 - secondary coil 1 and 2 have 10 turns each.

Load Coil The load coil has 900 turns in total with a calculated self-inductance of 13.5 mH. This was calculated by assuming that there were 30 layers each with 30 turn, an inner diameter of 14 mm and 11 mm in length.

Wiring of the Secondary Circuit For the secondary circuit (switches, load coil and secondary coils) the wiring is made from Nb25Zr (Niobium and Zirconium).

The Switches Acting as the superconducting switches were two 0.5 kΩ resistors that are 'glued' to the superconducting wire by stycast. When a current passes through the resistors they will heat up and break the superconductivity of their respective circuit loop acting as switches which can "open" and "close" the circuit. Like the coil, the two switches are covered in epoxy. The resistance R of the loops in normal state resistance (ie. when the heaters are on) is estimated to be approximately 200 μΩ [4].

Two Aluminum Pressure Joints The pressure joints are an ingenious solution for connecting wires and avoiding relatively high resistances compared to the more conventional soldering of wires. Three wires meet per joint (with an additional dummy wire to optimize surface contact) are cold-welded together by the mechanical force of six socket screws tightened with a torque wrench of 60 Ncm.

Temperature Sensor A Cernox thin film resistance cryogenic temperature sensor (CX-1010) was used and placed between the load coil and the bottom right pressure joint. It measured the temperature in Kelvin scale.

Fluxgate Magnetometer A Barrington MAG-01H Single Axis Fluxgate Magnetometer was used to measure the magnetic field induced as a result of current present in the load coil. Either by means of experimental methods or from a theoretical calculation, it is possible to calibrate the measurement readings of the Fluxgate meter to correspond the load coil current. Unfortunately, the sensor would saturate at 590 μT.

[3] The use of a Vespel polyamide core was a design improvement by Evens. V2.0 used an aluminium core that induced eddy currents. In replacing the material of the core, Evens improved the self-inductance from 1.113 mH to 4.449 mH.

[4] This is based on the electrical resistivity of Niobium-Zirconium alloys at critical temperature (9.29 K) and assuming that only a small part of the loop becomes resistive [21].

3.2.2 Flux Pump Circuit V4.0

Due to the limited range of the Fluxgate Magnetometer in measuring the load coil's current, another magnetic field sensor was required in order to characterize the flux pump circuit.

Several external sensors were trialed and yet failed to measure the magnetic field outside of the cryostat due to the magnetic field being too weak. Hence it was determined that a Hall Sensor should be used.

It should be noted that in van den Berg's V2.0 flux pump circuit, a Hall sensor was used. However, it was placed in full thermal contact with the load coil whereas the load coil was only partially isolated from the copper ground place. Thus, when the Hall sensor was in operation, it would heat up the load coil through Joule heating breaking the superconductivity of the load coil.

Figure 3.2 is a schematic drawing of a support apparatus that could hold both the Fluxgate meter and the Hall sensors. The Hall Sensor was glued to the underside of a copper beam that was supported by two aluminium poles. The Hall Sensor lied directly above, although not touching, and along the vertical axis of the load coil. Of course, when in operation the Hall sensor will still heat up but this was compensated for by a having a thermal contact between the copper beam and copper plate – thus manipulating the heat away from the load coil. For calibration purposes, the Fluxgate meter remained in the cryostat chamber but this time directly above the Hall sensor supported by a second copper beam.

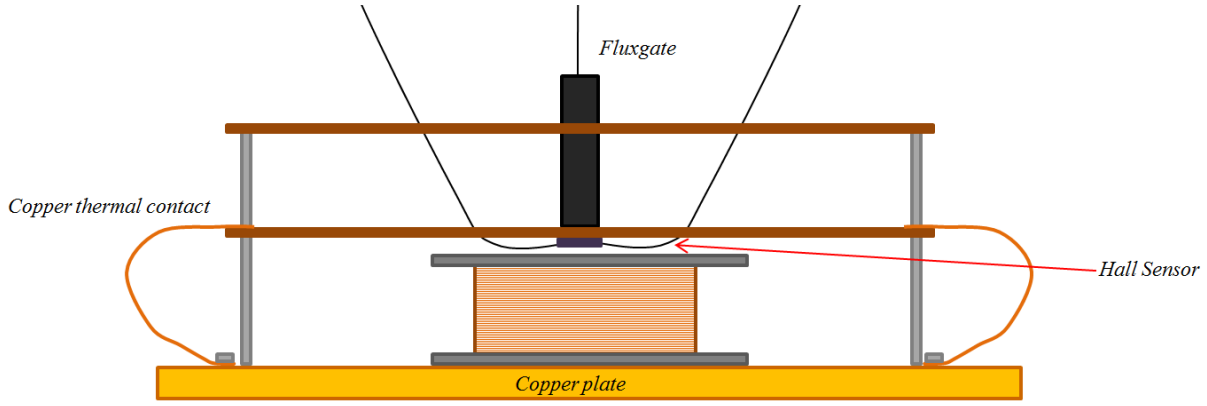

FIG 3.2 Hall sensor and fluxgate meter support apparatus for flux pump circuit V4.0.

3.2.3 The Cryostat

The flux pump most operates in superconducting conditions which is achieved by means of a cryostat. The circuit was mounted onto a copper ground plate which was attached to the base of the cryostat for good thermal conductivity, which allows for better cooling of the superconductive components.

A schematic drawing of a two stage cryostat is shown below (Fig. 3.3). The chamber is thermally isolated from room temperatures by creating vacuum chamber. The "two stage" refers to using liquid nitrogen in the outer chamber (having a temperature of 77.3 K) and liquid helium in the inner chamber (approximately 4 K) in order to reduce the helium boil off rate.

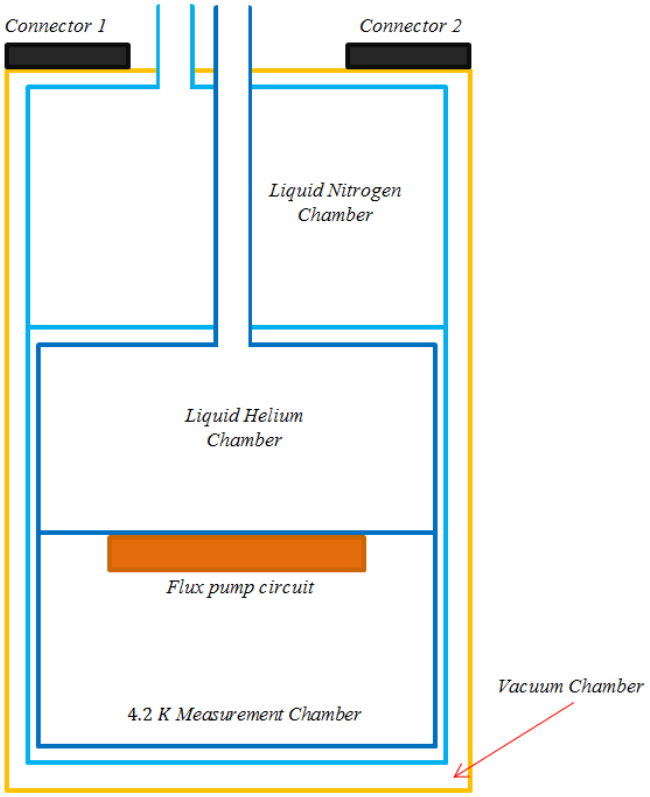

FIG 3.3 Schematic drawing of the cryostat used.

3.2.4 The Cryostat Wiring

The cryostat has two female DB25- 25 pin connectors that correspond to the two male DB25 connectors on the outside of the cryostat. Linking the two connectors is Manganin wire which has roughly 40 Ω per wire and a low thermal conductivity relative to copper.

Via a female-to-male convertor, the various wires of the measuring components and circuit elements are soldered to the connectors. Connector 1 (see fig. 3.4) uses 20 pins in order to supply current to the primary coil. They are soldered in such a way that there are 20 parallel wires (10 each for the negative and positive power supply) giving an effective resistance of approximately 8 Ω. The benefit of this is twofold, it allows for larger currents to be injected into the circuit whilst reducing the heat dissipation compared to if a single wire was used.

Also connected to connector 1 is the Fluxgate meter. Connector 2 serves as the port for the remaining components and sensors. For a complete overview of the all the connections and additional comments on the flux pump/ cryostat wiring, please refer to appendix 7.a.

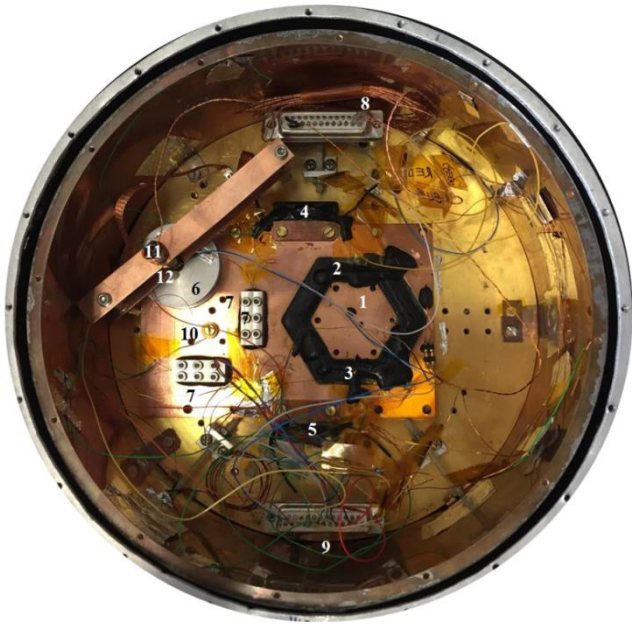

FIG 3.4 Labeled picture of the flux pump circuit V4.0.

1.	Primary Coil	7.	Pressure Joints
2.	Secondary Coil 1	8.	Connector 1
3.	Secondary Coil 2	9.	Connector 2
4.	Heater Switch 1	10.	Temperature Sensor
5.	Heater Switch 2	11.	Fluxgate Meter
6.	Load Coil	12.	Hall Sensor (not visible)

3.2 Outside the Cryostat

One of the most tedious and time consuming parts of the experimental setup was collaborating and testing the external equipment that supplies and measures the internal elements of the cryostat. Again, credit is due to van den Berg's report for providing a good starting point to wiring and setting up the necessary equipment.

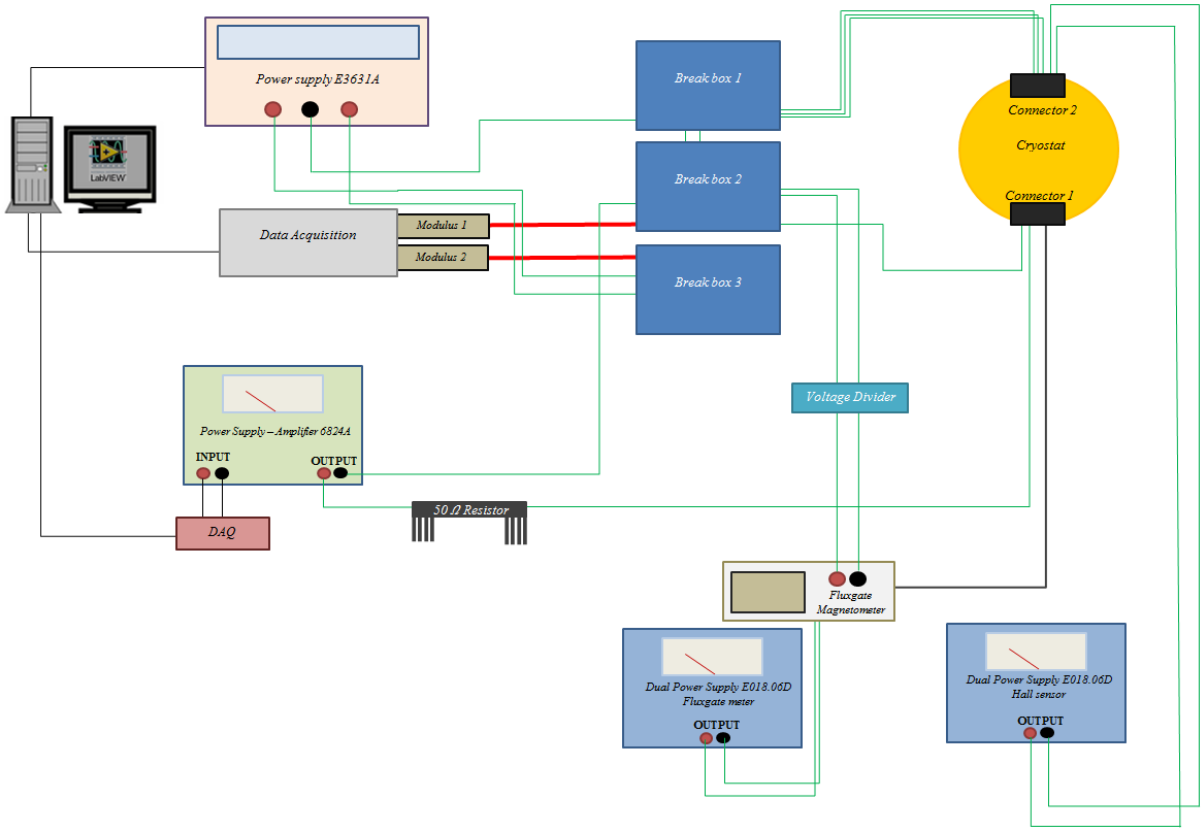

FIG 3.5 A schematic drawing of the external experimental set-up.

A schematic drawing of the external experimental set-up including the computer, which contains the LabVIEW software that us used to control and log all parameters, is shown above (see Fig 3.5).

Starting with the elements that are associated with connector 1, the primary coil current is controlled by the LabVIEW software. Setting a desired current value into LabVIEW, the primary signal is generated by the DAQ module after which it is amplified by a factor of 10 by the Harrison 6824A Power Supply Amplifier. A 50 Ω resistor is placed in series with the amplifiers output before the signal enters the cryostat via connector 1 - allowing the signal to pass through break box 2 allows for it to be monitored by the LabVIEW program. An E018-0.6D Dual Power Supply powers the measuring unit of the fluxgate meter and via connector 1, this unit receives information from the fluxgate meter probe inside the cryostat. To adjust the sensitivity of the Fluxgate meter, the output signal is modified via a voltage divided before passing through Break box 2 and be logged by the 34970A Data Acquisition/ Switch Unit.

The input and output signals of all other various elements inside the cryostat are connected to connector 2. The Hall sensors are powered by an E018-0.6D Dual Power Supply. The other elements pass through Break Box 1, before being ordered and sent to Break Box 2 and then logged by the Data Acquisition Unit. The heater currents are generated by the E3631A Power Supply and pass through Break Box 1 before being sent into the cryostat. The Data Acquisition Unit processes the electrical data before sending it to the computer.

For a complete overview of the all the connections, wiring, operation and additional comments on the external set-up, please refer to appendix 7.a.

3.3 Digital Interface - LabVIEW

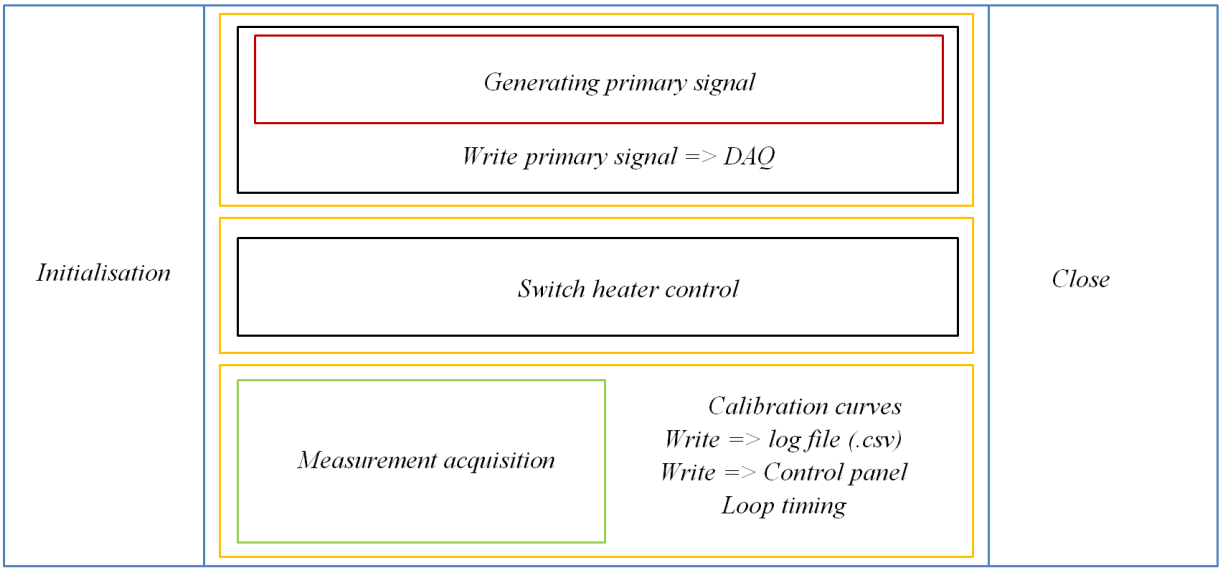

FIG 3.6 Visual representation of the LabVIEW program structure.

The schematic above (see Fig 3.6) is a representation of the LabVIEW program structure with different coloured boxes representing loops in the program.

Starting from the left, the initialization section is responsible for resetting, configuring and storing data from the controlled instruments.

Looking at the top of the middle section, the "Generating primary signal" module quite literally generates a signal based on the settings in the control panel and is turned on by the use of a start button reading 'primary signal on'. The middle module "Switch heater control" controls the thermal switches from which you can set the heater current limit. The "Measurement acquisition" module in the bottom middle loop, collects processes and stores measurement readings from the data longer as well as collecting parameter values and timings from the control panel and control loops. Calibration curves are automatically applied to temperature sensors converting the reading into its appropriate units. The measurement timing is set by a wait in the loop. The length of this wait must be longer than the time required collecting all measurement readings in one iteration.

3.3.1 Generating the Primary Signal

Figure 3.7 shows the user interface for setting the primary signal wave. Please refer to appendix 7.b to view the formula node script that generate the primary waveform using the parameters listed below.

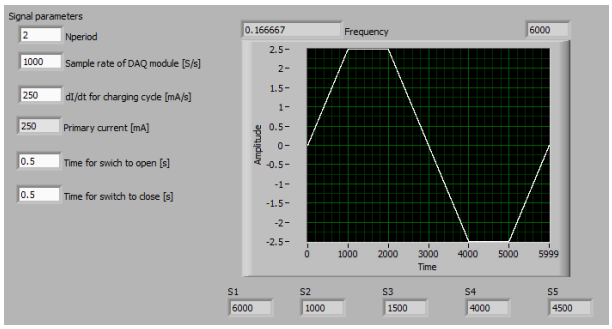

FIG 3.7 Screenshot of the control panel of V3.0 LabVIEW program that sets the generating primary signal.

Nperiod – Corresponds to the number of half cycles. This should, at all times, be set at 2 in order to generate a full wave,

Sample rate of DAQ module [S/s] – This rather self-explanatory title is the parameter that controls the number of samples you want the DAQ unit to measure per second – 1000 samples per second is satisfactory.

dI/dt for charging cycle [mA/s] – Is the rate of change of the primary current with time. For the sake of simplicity in determining the frequency, primary current was such set such that it would reach its peak value, regardless of the magnitude, in 1 second.

Primary current [mA] – The peak primary current value - I_P.

Time for switch to open [s]/ Time for switch to close [s] – These two parameters consider the time required for the thermal switches to heat up and cool down in order to break and regain the superconductivity of each loop. They correspond to how long the primary signal remains constant at peak value I_P. The optimal value of these parameters can be determined experimentally by adjusting the frequency of the primary signal.

3.3.2 Controlling the Heaters

The current sent to the thermal switches can be set in the control panel as shown in figure 3.8. It is preferable to make this value as small as possible to minimise heat dissipation whilst ensuring it is large enough to break the superconductivity of either loop in a reasonable time.

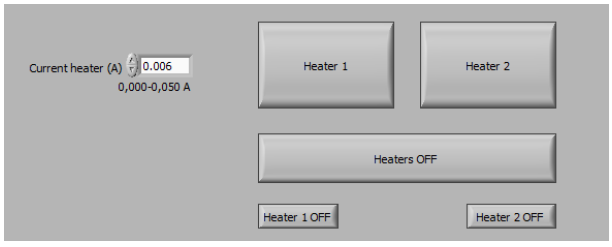

FIG 3.8 Screenshot of the control panel of V3.0 LabVIEW program that sets the heater current.

3.3.3 Inductive Communication Wave

Some changes were made to the LabVIEW program in order to test inductive transfer in the flux pump circuit –figure 3.9 is a visual representation of the changes made. The new parameters are listed as below.

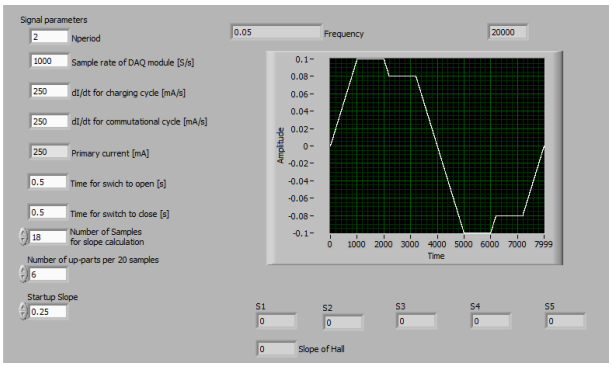

dI/dt for commutational cycle [mA/s] – This is the rate of change of the current step. It is set to the same rate as charging cycle.

Number of Samples for slope calculation/ Number of up-parts– These two parameters correspond to the magnitude of the current step decrease. As outlined in the theory, the step decrease should be of equal magnitude to the increase of current in the load coil. Due to one of systematic errors where the current in load coil does not increase, the LabVIEW program takes the total current increase over a "Number of Samples" and divides that value by the "Number of up-parts". For example, if the number of sample for slope calculation was set to 18, the number of up-parts would be set to 3.

4 Results and Discussion

The results and discussion are divided into 5 sections – testing V3.0 of the flux pump; calibrating the sensors; testing for the optimal primary wave; charging the load coil to saturation, power and efficiency analysis and the failing of the circuit.

4.1 Testing V3.0 of the Flux Pump

To test the functionality of the flux pump, some repeated experiments were performed on V3.0 of the flux pump.

4.1.1 Pumping V3.0

Shown below, graph 4.1 shows the experimental data of the load coil current as a function of time.

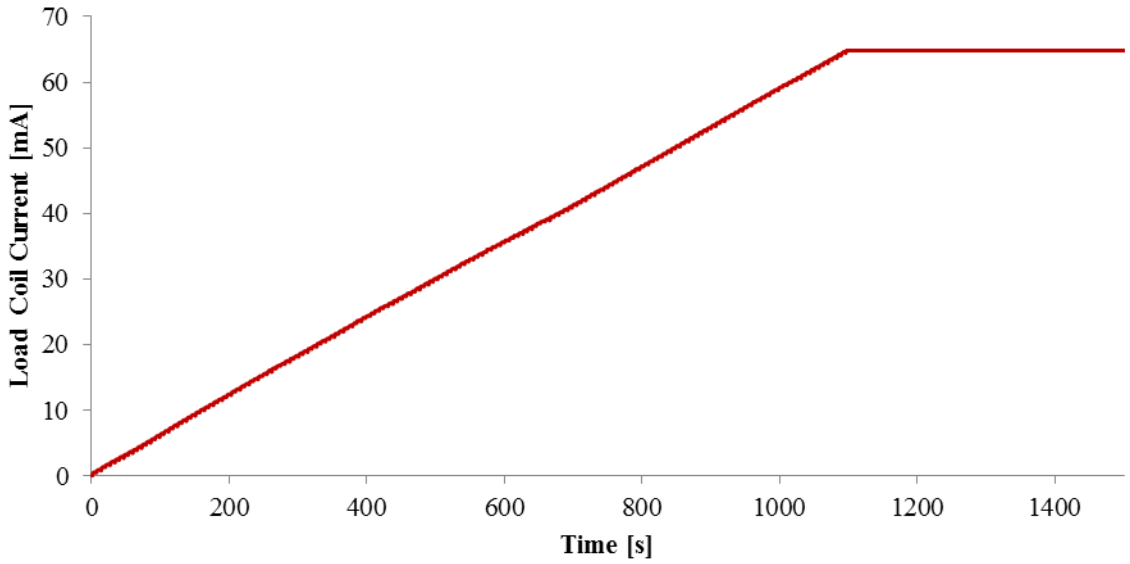

GRAPH 4.1 Initial flux pumping operation with a high primary current (125 mA). At 60 mA, the magnetic field strength of the load coil is larger than the range of the fluxgate meter.

The current increases initially as a function of time in a linear manner until the magnetic field strength of the load coil surpasses the range of the fluxgate meter. Although what graph 4.1. does show is an increase in load coil current, due to the limited data one cannot characterize or analyses this flux pump system. According to equation (13), it is expected that the load coil current rises exponentially which the data presented in graph 4.1 seems to defy. A logical reason for this being could be because the range of the

data measured is insignificant compared to the total theoretical exponential curve. One could argue that any increasing trend line could be manipulated to look linear if one focused on only a small sample of the data.

None-the-less, the data presented in graph 4.1 is insufficient to characterize this flux pump system. However, it does show that the flux pump is working.

4.1.2 Persistent Current Test

In this experiment, the load coil was pumped up to approximately 10 mA before switching of the primary signal and the operation of the heaters. The temperature inside the cryostat and as well as the load coil current were monitored over a 12 hour period. Data showed that the load coil current remained constant over the full run of the experiment – with absolutely no significant decrease in current.

This experiment proves that a persistent current can be maintained inside the load coil so long as the circuit remains superconducting.

4.2 Calibration

As mentioned, an additional sensor was required in order to analyses the flux pump system.

Initially trailed was a Barrington MAG-03MS100 Three-Axis Magnetic Field Sensor and a Hand-held Gauss/ Tesla Mater Model 4048 both with a significantly higher range. Both were tested underneath the outside of the cryostat in line to measure the magnetic field strength along the axis of the load coil. The idea was to sense a change in magnetic field outside the cryostat due to the load coil current. However, at this stage in the project, little was known about the behaviour of the load coil and the current it could hold. Furthermore, the magnetic field strength along the decreases rapidly outside the length of the solenoid [16]. So unless, without actually being able to measure it, the load coil built up a significant current; using the two mentioned external field sensors was unreliable and clumsy. Hence it was determined that a Hall Sensor should be used.

In order to calibrate the hall and fluxgate sensor, a known current is sent through the load coil and the response of each sensor is used to calibrate them respectively.

With a power supply sending connected via pins 8 and 20 on break box 1, a current could pass through the load coil. Both switches 1 and 2 remained on during this calibration process. This ensured that the current passed through the load coil instead of simply travelling through the low resistant superconducting loops.

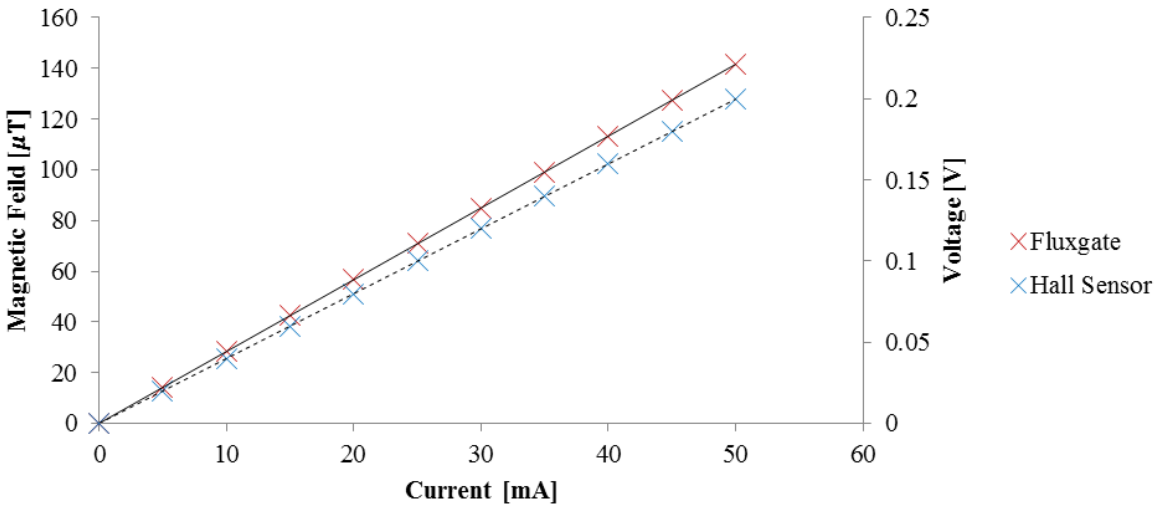

GRAPH 4.2 Showing the response of the Fluxgate meter and Hall sensor with changing current.

Both the fluxgate and the hall sensor have a linear response to the changing current in the load coil – which is to be expected as the magnetic field of an inductor is directly proportional to the current.

By calculating the gradient of each graph, a correlation between the output of each sensor and the current of the load coil can be determined. For the fluxgate meter the relation is 2.83 μT/mA and for the Hall sensor the relation is 0.004 V/mA.

In order to test the relation between the fluxgate meter and the Hall sensor, one can test the linear response of the two sensors.

Graph 4.3 plots the normalized output response of the fluxgate meter and the Hall sensors.

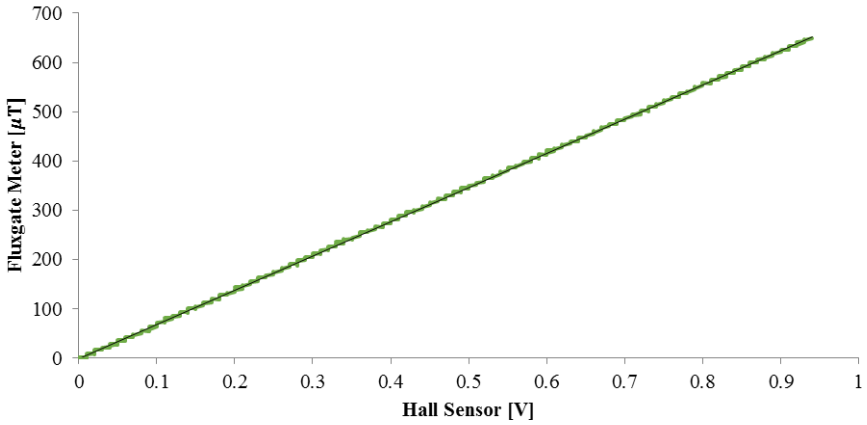

GRAPH 4.3 The output response of the Hall sensor and the flux gate meter are plotted against each other producing a linear line of best fit.

As expected, there is what appears to be a perfect linear fit between the responses of both sensors. For future reference, the relation between the Hall and Fluxgate sensor is 0.00145 V/μT.

4.2.1 The Sensors Dependency on Temperature

During long experimental runs, it is expected that the temperature will slowly increase with time due to helium/ nitrogen liquid boil off. Both the hall sensor and fluxgate meter have a temperature coefficient and specified operating temperatures. Thus, to see the effects that temperature had on the reliability and sensitivity of the sensors, the following experiment was carried out.

With no current induced in the load coil, the output response of the hall sensor and the fluxgate meter was measured as of temperature. The data collected from this experiment is shown in graph 4.4[5].

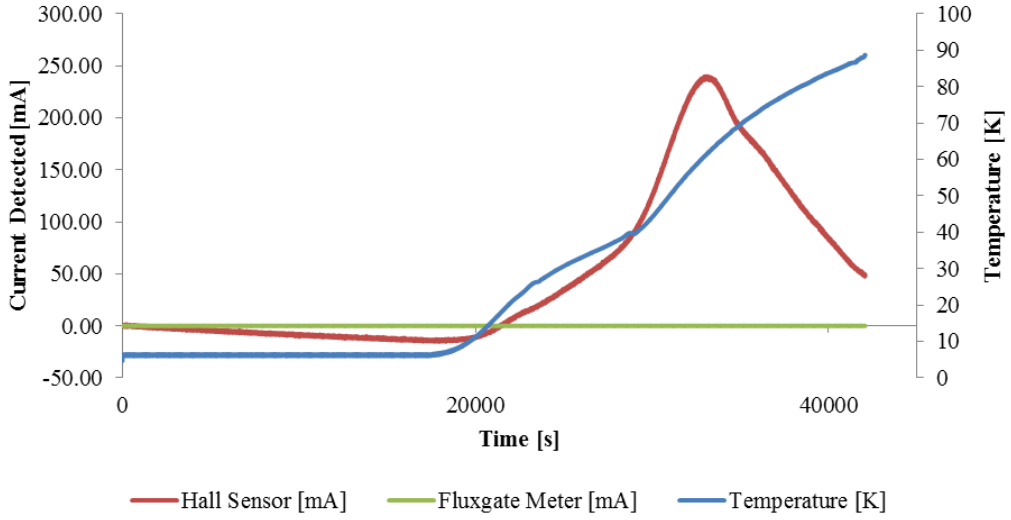

GRAPH 4.4 Offset current produced by the fluxgate meter (green line) and the hall sensor (red line) as a function of time, as well as the temperature (blue line).

It is clear from this data that the output of the fluxgate meter is not affected by an increasing temperature, for which the same could not be said about the hall sensor. Whilst the temperature inside the cryostat remains relatively constant (due to the presence of liquid helium), the output of the hall sensor gains a negative offset (reaching a minimum value of 15 mA) up until the point where the liquid helium has totally evaporate increasing the rate at which the temperature rises. When the temperature is approximately 60 K, the hall sensor gains a positive offset of significant value – approximately 240 mA.

The bizarre behaviour of the hall sensor begins to make sense when you consider the operation of a hall sensor. In short, when a hall sensor is placed within a magnetic field the magnetic flux lines exert a force on the semiconductor material which deflects the charge carrier (electron and holes) to either side of the semiconductor slab [17]. As these electrons and holes move side wards a potential difference is produced between the two sides of the semiconductor. It is this measurable potential difference that allows a Hall sensor to measure magnetic fields. Now the charge carrier density depends on the temperature, thus if the

[5] The date presented from the Hall sensor and the flux gate meter has been adjusted to realise the presence of the Earth's magnetic field. The magnetic field was converted into current using the information extrapolated from graph 4.2. This is the case for all remaining data in this report.

temperature is increasing carrier density will also increase explaining when such a large offset peak occurs in graph 4.4. However, this explanation does not account for the negative minimum that occurs.

Luckily, for the purpose of this experiment where we are only interested in temperatures below 6 K a maximum negative offset of 15 mA will prove not to be too damaging to future measurements in the grand scheme.

4.3 Testing the for the Optimal Wave

One of the research questions in the report focuses on the efficiency of charging the flux pump circuit.

4.3.1 Finding the Optimal Frequency

In order for any flux pump system to charge in the shortest amount of time, equation (13) predicts that the higher the frequency of the primary signal the faster the flux pump will reach its limiting value. However, if the frequency is too rapid, then thermal switches will not be able to cool and heat up in time and the system will simply not work.

For this experiment, a range of frequencies were used for the primary signal as listed in table 4.1.

Table 4.1 Lists the trialed frequencies along with comments on their performance.

Frequency [Hz]	Working	Comment
0.250	No	Frequency too fast, heaters could not cool/ heat up in time
0.200	Not reliable	
0.167	Yes	Ideal
0.143	Yes	Too slow
0.125	Yes	
0.111	Yes	

The information presented above is in agreement with what was predicted. For the lower frequencies, 0.111 Hz – 0.143 Hz, the flux pump circuit does work, however it would take a very long time for the system to reach its maximum load current. For the highest frequency, 0.250 Hz, the system does not work as the heaters can't keep up with this frequency. For 0.200 Hz the load coil current increases in a stagnated manner, resulting in the heaters working some of the time.

Thus, it can be concluded that, when considering the trade-off between charging rate and reliability, the ideal frequency for the primary signal is 0.167 Hz.

4.3.2 Finding the Optimal I_P

Again, referring back to equation (10) which dictates that the larger the primary peak current I_P, the larger the maximum current that can be induced in the load coil. It is clear, however, it is inevitable that a trade-off will arise between the maximum primary I_P and reliability of the system.

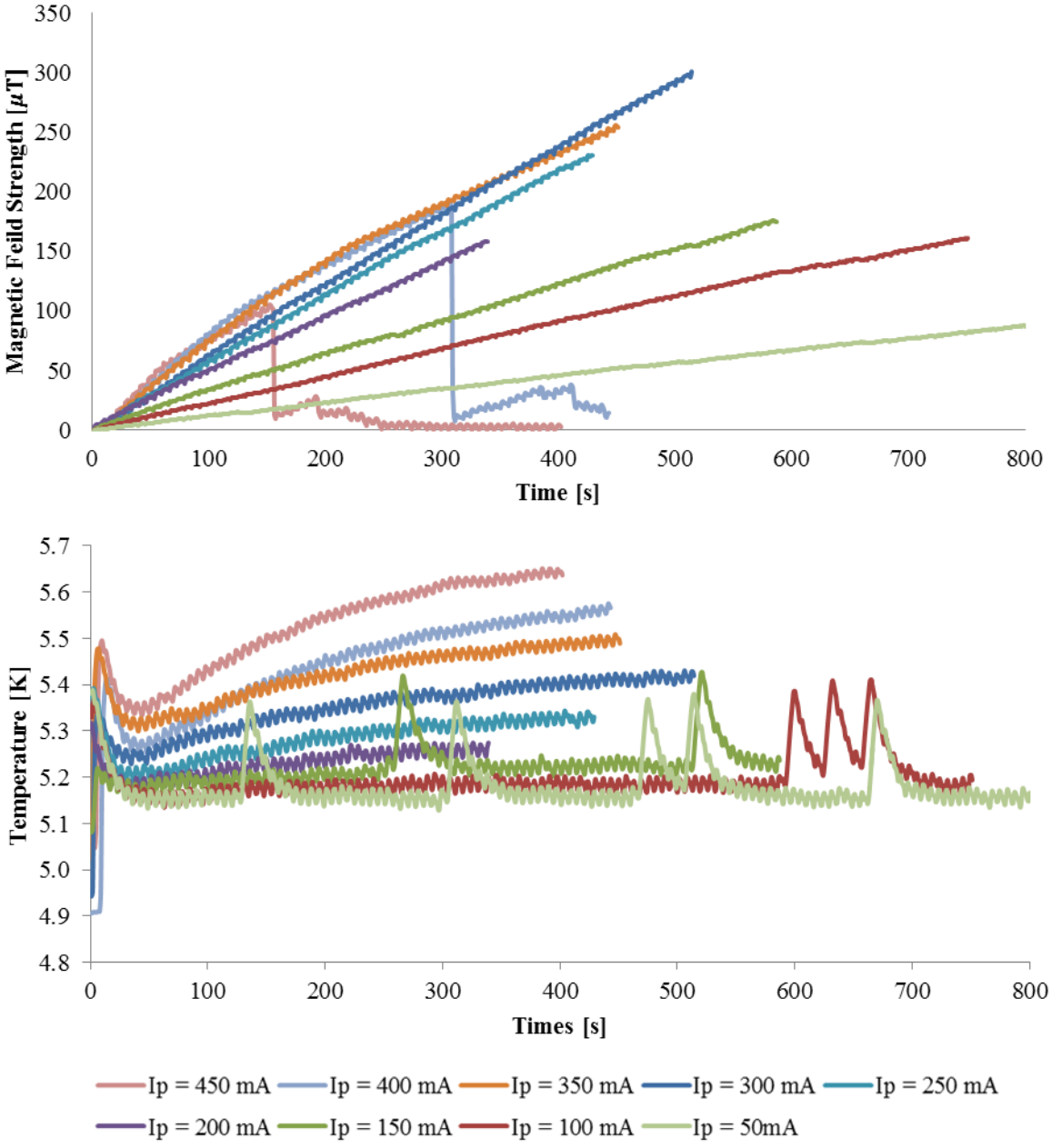

GPAPH 4.5 (a) & (b) The top graph (a) shows the magnetic field strength produced by the load coil current for various primary currents. The bottom graph (b) shows the corresponding temperature inside the cryostat during the pumping process.

Looking at the light green data line which represents a primary peak current of 50 mA, it is clear that the magnetic field strength of the load coil is increasing as a function of time - indicating an increasing load coil current. However, it has a very shallow increase and will produce the smallest maximum load coil current.

Looking to the maximum primary current of 450 mA represented by the pink line, initially the increase in magnetic field strength is the steepest of all the different value. However, at approximately 150 s into charging, the magnetic field strength drops. This is due to the circuit losing its superconducting state resulting in the load coil quenching because the temperature in the cryostat is too high. This also occurs when using a primary peak current of 400 mA and it looks like the same problem will occur when using 350 mA. Looking at the recorded temperature during these three values, we can approximate that when the temperature inside the cryostat approaches 5.50 K, superconductivity in the system will be lost and the flux pump circuit will not operate.

This represents the trade-off between the maximum current and the reliability of charging. Using a larger the peak primary current will increase the temperature inside the cryostat. If the temperature approaches 5.50 K, the flux pump will not work. On the other hand, a smaller peak primary current will decrease the maximum current obtainable in the load coil and increase the time required to get there.

According to equation (13), the load coil current is directly proportional to the peak primary current. This implies that doubling I_P will double I_L for any time t. Using the data from graph 4.5.a at 150 s, the rate of change was determined and plotted against the corresponding peak primary current – see graph 4.6.

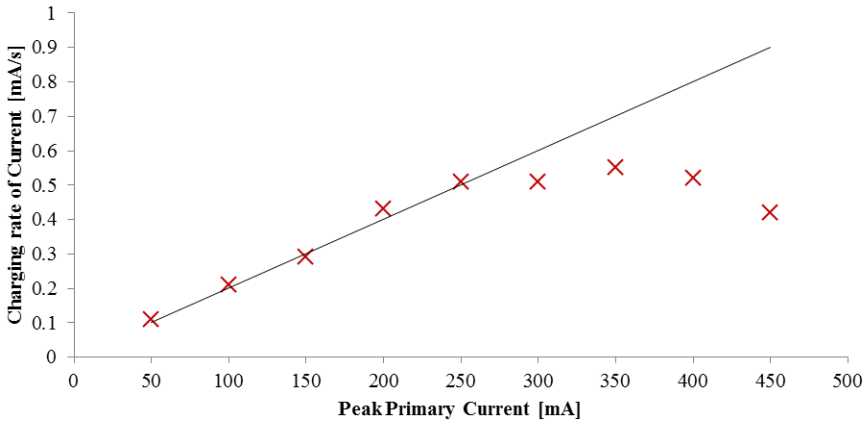

GRAPH 4.6 Charging rate of current at 150 s plotted against the peak primary current with a black trend line representing the expected result.

The black trend line in graph 4.6 represents the theoretical fit one should expect if the load coil current is charging correctly for each peak primary current. However, at 300 mA the experimental data begins to fall away from this line.

Thus, it can be concluded that, when considering the trade-off between peak current and reliability, the ideal amplitude of the primary signal is 250 mA.

4.4 Characterizing the Flux Pump System

Now that the optimal wave was determined for the system to charge reliably and as fast as possible, the next experiment was to charge the load coil until saturation.

Despite leaving the flux pump system to run over night and repeating this experiment three times, the current measured in the load coil never levelled off indicating the system had reached its limiting value. Graph 4.7 shows the data collected from the three attempts.

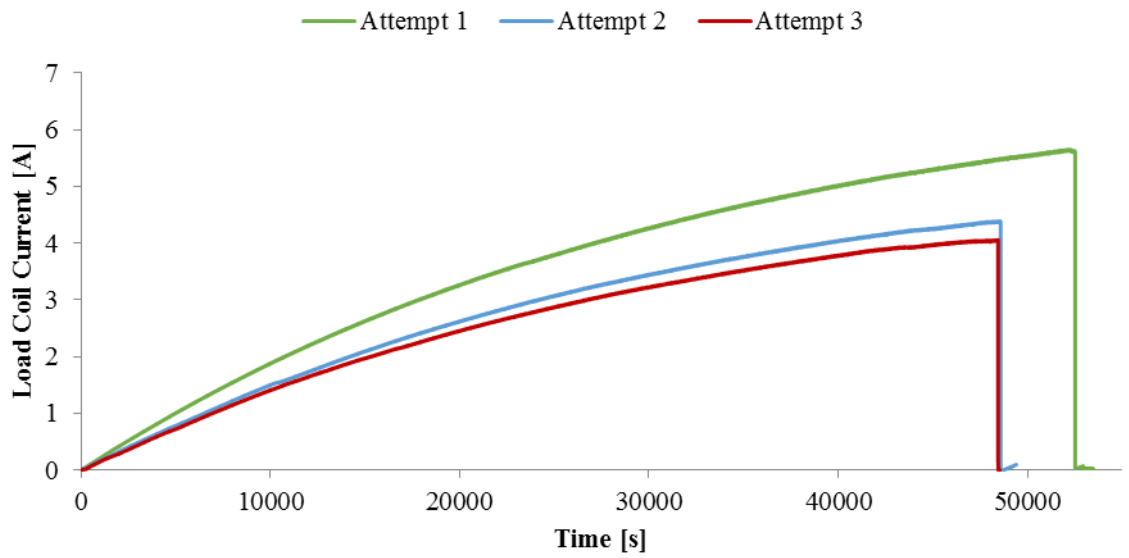

GRAPH 4.7 Shown above is the load coil current as a function of time for attempt (green), attempt 2 (blue) and attempt 3 (red). Not the sudden drop in current for each of the curves, this is the load coil quenching.

For all three attempts, the load coil quenches resulting in the sudden current loss[6]. For attempts 1 and 3, the liquid helium inside the cryostat had evaporated resulting in a rapid increase in temperature. For attempt 2, heater 1 remained "stuck" for a significant amount time increasing the temperature inside the cryostat resulting in the circuit losing its superconductivity [7]. It should be emphasized that despite the load coil quenching at a similar time for attempt 2 and attempt 3, this is purely coincidental and (to be the best of my understanding) provides no useful information about the behaviour of this flux pump. See the temperature graphs in appendix 7.c as evidence.

Despite the mentioned "failures" above, a lot of information can be extrapolated from graph 4.7. to characterize this flux pump system.

[6] ***Do not worry!*** For attempt 1, where the largest current of just under 6 A in the load coil was measured, the total energy released in the dissipation of the load coil was 0.25 J. So please do not think that the cryostat exploded like a stick of dynamited as suggested in the theory – this requires kilojoules of energy!
[7] The cause of heater 1 being "stuck" is a software/ programmatic problem caused by some kind of timing bug.

First of all, for all three attempts the increase in the load coil current is different for each run. In case it isn't already clear, absolutely all experimental parameters were the same for each attempt – this included the amplitude and frequency of the primary signal, heater current and initial temperature of the cryostat. Logic suggests that there should be no significant difference in the experimental results for each run, yet the charging rate gets lower and lower and the exponential increase gets shallower and shallower. This unexpected behaviour hints towards a certain lack of reliability in this particular flux pump. Naturally, it is undesirable for a flux pump to behave in a different manner every time it is charged. To understand why this is happening, one must consider a couple of possibilities:

Wear and tear The act of frequently cooling down and heating up the cryostat between cryogenic and room temperatures could have a negative effect on circuit in the cryostat. When cooled down, all elements will shrink and when heated, return to their original size. It is easy to imagine that this compression/ expansion reputation will take its toll on some of the circuit elements. The self-inductances of the four load coils used are vital in determining the behaviour of the flux pump, if their respective coils are altered or damaged in any way during changing temperature this would influence how the flux pump will operate.

Can't handle the charge The wiring used for the load coil, being superconducting, is incredibly thin. It could be that when the coil quenches and the current is dissipated, these thin wires can burn-out or short circuit. This would reduce the effective number of turns in the load coil which would also reduce its self-inductance.

Now one might argue that according to equation (10) the self-inductance of the load coil has no effect on the limiting current, so it can't the load coil that is failing. This is true; however, the load coil current is an indirect measurement. The Hall sensor and the fluxgate meter are not ammeters, their magnetic field sensors. So if the load coil is short circuiting and the number of turns is decreasing, the magnetic field strength that the load coil will produce also decreases [18]. This means that relation between the load coil current and output of the sensor (the Calibration experiment – 0.004 V/mA for the Hall sensor) is no longer valid. Hence, explaining why the load coil current is decreasing.

Pressure joints under pressure Again, the pressure joints which connect the thin superconducting wires may be damaged when the coil quenches. Thus, for during the next charging cycle, more power is loss through these joints affecting the charging rate of the load coil.

4.4.1 Fitting a Theoretical Model

Taking attempt 1, as it assumed to be the most 'reliable', the experimental data was plotted with a theoretical fit of the flux pump as shown in graph 4.8. The theoretical model was calculated by using the known dimensions of the various inductors as specified in the experimental set-up (page 22). The couple coefficient k_{PS} was taken from Even's report where he speculated a value of 0.42. Listed below in table 4.2 is a summary of the calculated theoretical inductances and other parameters.

TABLE 4.2 List of theoretical parameters

Parameter	Value
k	0.42
$\hat{I}_P$	250 mA
$L_S = L_{S1} + L_{S2}$	0.5 μH
L_P	4.45 μH
L_L	13.5 mH
f	0.167 Hz

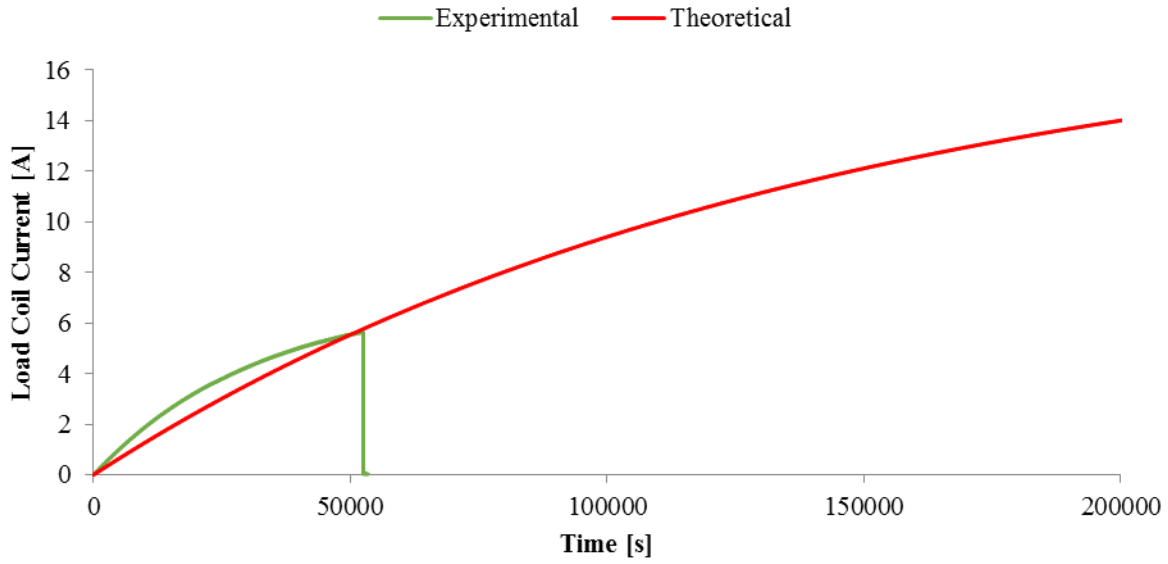

GRAPH 4.8 The experimental data (green) compared to the theoretical model (red).

Clearly, the experimental data doesn't fit the exponential curve described by the theoretical model. Perhaps this doesn't come as too much of surprise – we have already observed that certain elements change their characteristic after each run so it is justified to be sceptical of the theoretical values presented in table 4.2.

None-the-less, the experimental data does, as for all three attempts, show promise of an exponential increase. Without doubt, it can be said that this flux pump system does work however it can't be characterized by the predicted parameters.

4.4.2 Fitting the Experimental Data

To understand the behaviour of this flux pump further, from the experimental data certain parameters were extrapolated so that the theoretical equation (13) would fit. Certain assumptions were made regarding the trustworthiness of certain parameters. Both the frequency f and the primary peak current I_P are parameters that are set by the user so are taken to be true. From graph 4.7 it is clear that the limiting value of current decreases for every attempt. For the sake of fitting the experimental data, it is assumed that the load coil did not shirt circuit and that the load coil L_L is a reliable parameter. The self-inductance of the primary coil L_P was also measured using a LRC-meter by Even and was in strong agreement with its theoretical prediction, thus is also deemed fairly reliable. This leaves the coupling factor k_{PS} and the self-inductance of the two secondary coils L_S to be the values extrapolated from the experimental data. The theoretical model fits can be seen in graph 4.9.

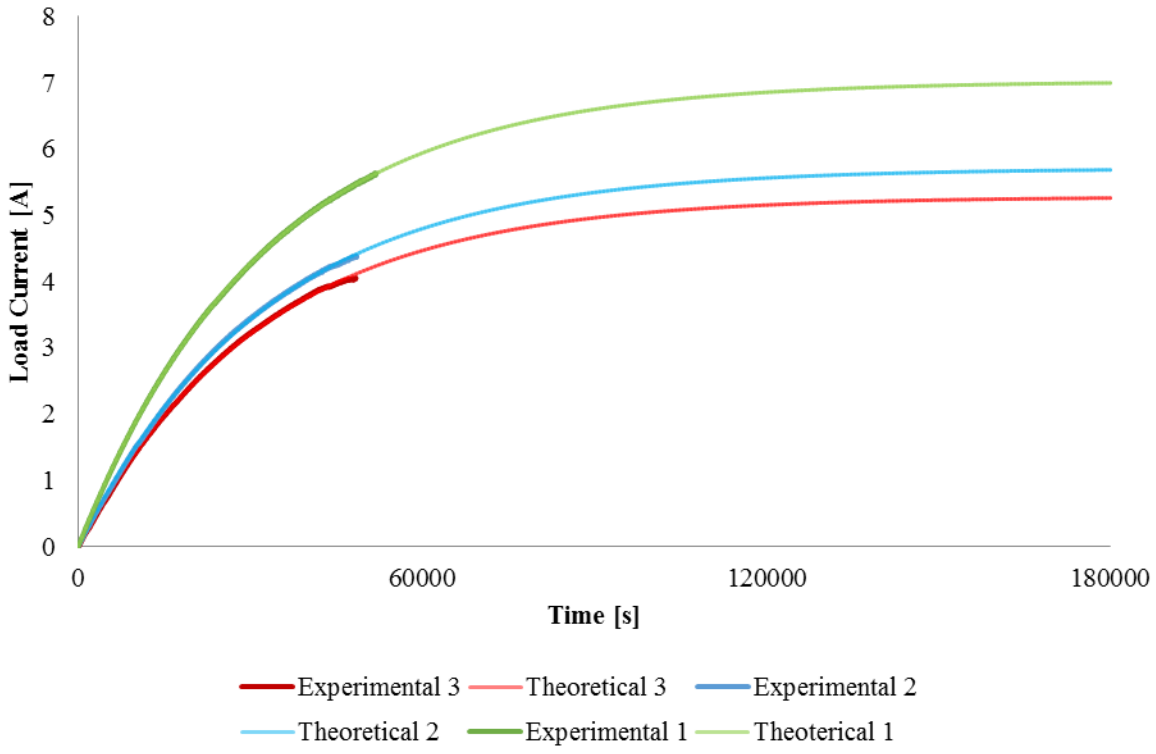

GRAPH 4.9 Each of the three experimental runs are given their own fit according to the theoretical equation (13).

For all three experimental attempts, a satisfying theoretical fit was obtained. Listed below in table 4.3 are the parameters that were extrapolated, the limiting load coil current (using equation (10)) and the maximum field strength produced by the load coil once charged [18].

TABLE 4.3 Extrapolated experimental parameters k and L_S, as well as the limiting current and maximum produced magnetic field, compared with the theoretical values.

	Attempt 1	**Attempt 2**	**Attempt 3**	**Theoretical**
k	0.24	0.19	0.18	0.42
L_S [μH]	1.26	1.24	1.26	0.58
$I_L^{(\max)}$ [A]	7.02	5.71	5.29	18.39
$B_L^{(\max)}$ [T]	0.73	0.59	0.55	2.19

Looking at the information provided in table 4.3, one can notice there seems to a factor of two missing from the experimental values in order to match that of the theoretically predicted values. For the sake of clarity, looking only at the extrapolated experimental parameters of attempt 1, the coupling coefficient is approximately half of the theoretical value. Whilst the self-inductance of the secondary coil is just over the theoretical value doubled. It could be pure coincidental that there is this factor of two missing in order to multiply or divide the theoretical values to match the extrapolated experimental values of attempts 1.

In order to achieve the extrapolated experimental self-inductance of attempt 1 using the theoretical equation (13), one can either double the length of the inductor, uses 15 turns instead of 10 or double the cross-sectional area. Even though there may be imperfections and errors present in the construction of the secondary coils, it is hard to believe that one would accidentally double the length its length without taking notice.

The self-inductance of the secondary coil is a similar value for each attempt. The same cannot be said about the coupling coefficient as, after each run, it gets smaller and smaller. It is disappointing that the coupling coefficient is very low considering that a hexagonal shaped primary coil was used for the sole reason it would reduce stray magnetic fields and improve coupling between the secondary and primary coil. The coupling coefficient does depend on the self-inductances of the secondary and primary coils. As we have already established, the secondary coils self-inductance is much larger than what was theoretically predicted. Therefore, one could argue that perhaps the primary coil is behaving in unexpected ways also. Despite the self-inductance of the primary coil being measured experimentally and producing the same value as what was theoretically determined, this was over a year ago. If we have already introduced the idea that this flux pump circuit is vulnerable to wear and tear, it could be that the primary coils self-inductance is no longer what it used to be.

As a matter of fact, this could be said for all elements in the circuit. The reason the coupling coefficient and the self-inductance of the secondary coil were chosen to be extrapolated was because this was the most logical deduction – it isn't guaranteed that these are the elements that are being altered, it could be all of them.

4.5 Power and Efficiency Analysis

4.5.1 Power Analysis

Using the experimental data of attempt 1 (as well as the corresponding extrapolated parameters), the power loss in the thermal switches and the power input into the load coil are plotted as function of load coil current in graph 4.10.

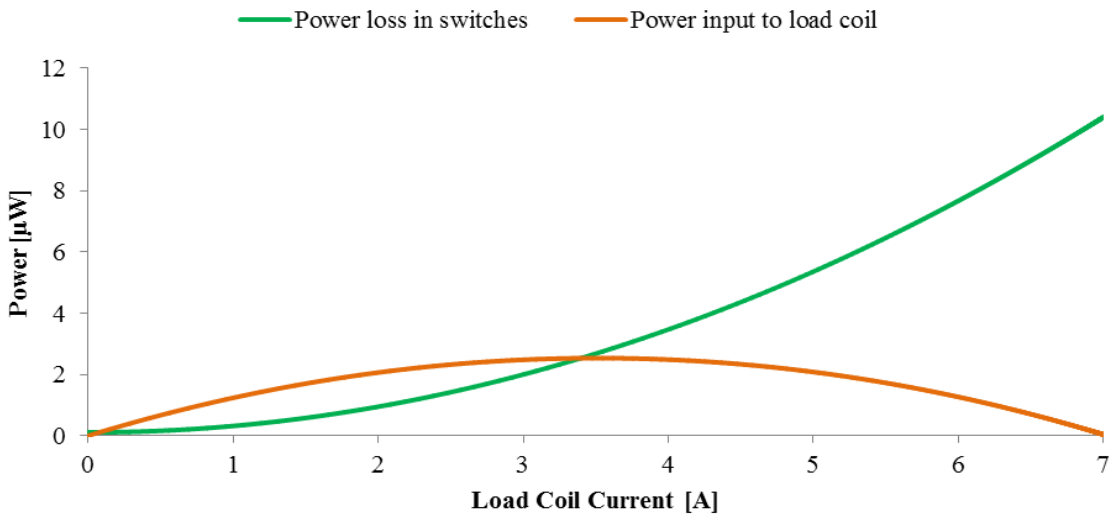

GRAPH 4.10 Power losses in the switches (green) and power input to the load coil (orange) as a function of load coil current.

The data presented above provided interesting characteristics this flux pump system. Looking at the power input to the load coil, it has a parabolic shape with its maximum at half the value of the limiting current ($I_{Load}^{(\max)}/2$) - this is mathematically characteristic of any increasing exponential charge rate. Furthermore, looking again at equation (16)

$$P_{Load} = I_{Load}(t)L_{Load}\frac{dI_{Load}}{dt}$$

which obviously implies there to be zero power when $I_{Load}(0) = 0$ and again when $dI_{Load}/dt = 0$ once the coil in the load current has leveled off and reached its limiting value.

As for the power loss in the switches, when $I_{Load} = 0$ there is still an initial power loss (it cannot be seen on the graph 4.10) 0.1 μW. This is due to unavoidable losses during the pumping region, when the induced current in the secondary loops is impressed across the thermal switches when in non-superconducting state. The power loss increase is directly proportional to the increase in load coil current. This is to be expected as the larger the current in the load coil, means a larger amount of current being dissipated in the thermal switched.

4.5.2 Efficiency Analysis

The efficiency of this flux pump system can be easily defined as

$$\eta = \frac{P_{Load}}{P_{Load} + P_{Loss}} \times 100\% . \qquad (20)$$

Thus, taking the data of graph 4.10, one can plot the efficiency of the system as function of the normalized current as shown in graph 4.11. Also shown is the charging rate as well as a black dashed line symbolizing the limiting case of resistive transfer efficiency.

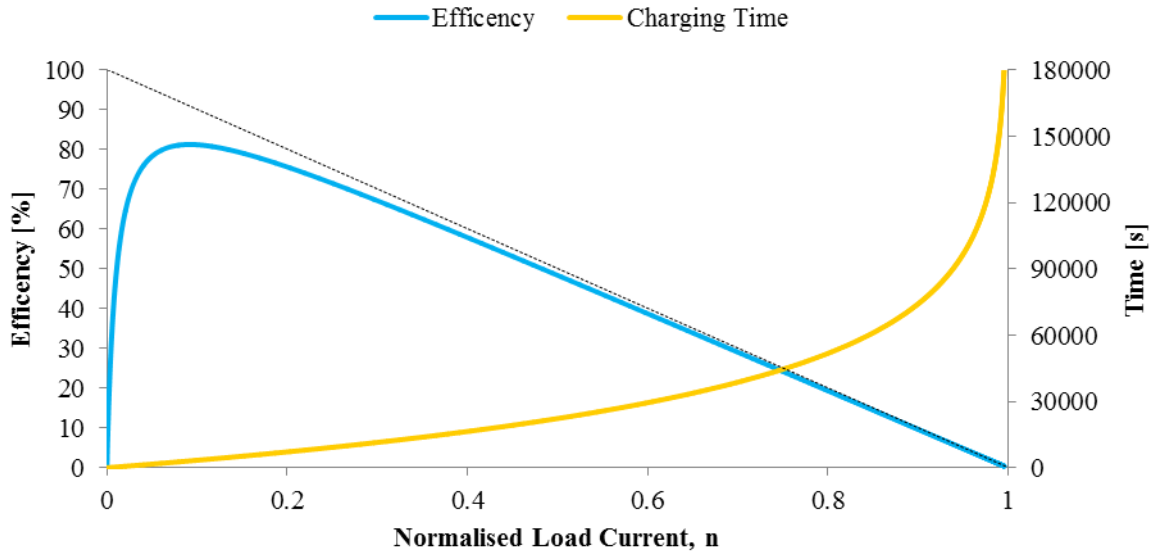

GRAPH 4.11 Efficiency and charging rate as determined by the data from attempt 1 as a function of normalised current.

The flux pump has a peak efficiency of approximately 80% when n = 0.1. Thus for maximum efficiency, this flux pump would have to operate at a current of 0.7 A – which isn't ideal. It is possible to alter the frequency of primary current to move the position of the peak at the cost of the maximum efficiency. Increasing the operating frequency will reduce the peak efficiency, but move the peak to a higher value of n. On the other hand, a reduction of frequency will increase the maximum efficiency, but will move the peak to a lower value of n. Resulting in a tradeoff between maximum efficiency and operating efficiency.

In order to improve the efficiency further, one could change the most important flux pump parameters that influence efficiency are the frequency, self-inductances of the secondary coil and the resistance of the thermals switches when in a resistive state. So an ideal flux pump would work at a very low frequency f, have a small secondary self-inductance L_S and a very high or infinite resistive state R. With $\frac{fL_S}{R}$ approaching zero, an energy efficiency of almost 100% is possible [19].

4.6 Experiment. Fail. Learn. Repeat.

As outlined in section 3.3.3, the LabVIEW program was altered in order to test the flux pump system during an inductive communication cycle. Unfortunately, it was never tested.

At one point, when the cryostat was cooled down, the flux pump failed to work for either inductive or resistive transfer. The cause seemed to come from the primary coil. When cooled down, the primary coil had an infinite resistance suggesting a break somewhere in one of its turns. However, when heated up again, the primary coils room temperature resistance was as expected - 17.45 kΩ.

It is bizarre that at superconducting temperatures, the resistance is infinite but at room temperatures it is normal. This implies that problem isn't caused by the primary coil (it is unlikely that two wires, once broken, will exactly re-join again), but aby a loose connection somewhere in the circuit.

To date, the exact fault hasn't been detected. The cryostat has been sprayed with cold gas and examined through a microscope, yet no sign of damage has been found.

5 Conclusion

Now, at the end of these three months, looking back at the research in its entirety – the procedure, the improvements, the failings and the results – the questions remains: Was it a success?

With some confidence, I can state that, to some extent, the research carried out in this report was a success. By furthering the work of van den Berg and Even, the performance of a flux pumping system was analysed including its stability, reliability, efficiency and the limiting current.

The following important results are evident from the analysis of the flux pump system.

1. This flux pump has an experimentally determined gain ($I_L^{(max)}/I_P$) of 29.
2. Both the maximum limiting current and the power input to the load coil are independent of the self-inductance of the load coil L_L.
3. Highest efficiency is obtained when with a large gate resistance, a low frequency and a low self-inductance of the secondary coil.
4. The system isn't very reliable as repeated experiments produce decreasing results.
5. Switching losses are an important factor in resistive transfer operation. Theory predicts that inductive communication is the preferred operating mode; however, unfortunately this was not tested.
6. There will always be multiple trade-offs when optimising the primary signal for a flux pump. It fundamentally comes down to a choice between high power input and high efficiency.
7. This experimental flux pump is capable of only low output energies (less than 1 J) and is not competitive with room temperature power supplies for energising superconducting load coils. However, flux pumps have been built to store energies of 10 kJ [20].
8. The total power used when charging is approximately 0.025 kWh.

5.1 Were all aims met?

Returning back to the research aims that were stated at the start of the report, the extent to which they were achieved is discussed.

Aim 1: Improve the sensing element for measuring the load coil current

At the start of this research, a load coil current of only 60 mA could be measured. Now, the measured current is one hundred times larger. Therefore, this research aim was met.

Even though a Hall sensor to detect the magnetic field strength was used before, the problem was it would heat up the load coil and break superconductivity. By designing and building an apparatus that could support a Hall sensor on axis just above the load coil, yet direct any heat generated away through thermal contacts, meant that an improved load coil current sensor was achieved.

The only negative points being the Hall sensors offset is affected by changes in temperature. This behaviour can be explained by considering the charge carrier density as a function of temperature. However, what is still unknown, that even at extremely low temperatures (below 10 K), the Hall sensor gradually produced a small negative offset even though the temperature remained relatively constant.

Aim 2: Determine the optimal primary wave for charging

The results gathered in this experiment symbolises the trade-offs that regularly occur when considering the operation of a flux pump. How quickly should the coil charge? How cold should the surrounding temperatures be? For the interests of testing the limits of this system, it was determined through data analysis, that the ideal primary wave should have amplitude of 250 mA and a frequency of 0.1667 Hz.

Aim 3: Measuring the load coil current until saturation

The data obtained from these experiments provides the most interesting and, to some extent, unexpected results. Running the flux pump until saturation was attempted three times, although it never made it due helium evaporation or heater 1 "sticking" and warming up the cryostat. Most unusual was the fact that the exponential curve changed for each attempt even though the parameters stayed the same. Through logical thinking and in-depth analysis, a few ideas were put forward to explain this anomaly. The most explanatory suggestion was that the effective number of turns in the load coil was decreasing due to wires short circuiting when the load coil quenched. This would reduce the strength of the magnetic field produced by the load coil and thus give the impression that the load coil current is lower than its actual value.

Furthermore, the experimental data was extremely inaccurate compared to what theory predicted. Both the rate of charge and the limiting current (experimental $I_L^{(\max)} \approx 7$ A and theoretical $I_L^{(\max)} \approx 18$ A) were extremely inaccurate. It was proposed that the reason of this was due the wear and tear of various elements.

To fit the experimental data, the self-inductance of the secondary coil L_S and the coupling factor k_{PS} were extrapolated such that the data would fit the theoretical model equation (13). The values obtained indicated that the flux pump system was capable of storing a current of $I_L^{(\max)} \approx 7$ (approximately 0.73 T) and would take 50 hours to reach saturation.

Recommendations for Improving Aim 3:

- In order to solve the problem of heater 1 getting "stuck". One may be brave enough to find the bug in the LabVIEW code. Alternatively, there are a range of alternative switches that could be used instead of thermal switches – such as magnetically controlled switches [20], although these may interfere with Hall sensor measurements

- Repeat the calibration method of the sensors (section 4.2) to check if, indeed, the detected magnetic field strength has decreased due to a reduction in the number of effective turns.
- In hindsight, the load coil is the circuit element that I believe to be causing the change in experimental data results. I would recommend fitting the experimental data, however this time extrapolating the load coils self-inductance and, from that, calculate whether or not the number of turns has decreased.

Aim 4: Perform a power and efficiency analysis on the flux pump circuit

Using the experimental data of attempt 1, the power and efficiency of the flux pump system was analysed. The results highlighted the power losses due to pumping and switching. Furthermore, the flux pump system exhibited a high efficiency of approximately 80% when the load coil current was 20 % charged. The efficiency drops to below 50 % when the load coil current is roughly 3.

Despite taking 50 hours to reach its limiting current, one must remember that when considering the possibilities of applying flux pumping technology for satellite application, the space missions will last months. So a long charging time is insignificant considering the current will remain persistent so long as the coil is superconducting.

5.2 Recommendations for Future Improvements

In terms of analysing this flux pump, there is limited work left to do.

It would be interesting to observe inductive transfer, however this would only improve the efficiency and decrease the charging rate time.

Another area of interest could be modifying the system to incorporate a secondary persistent current coil that can be used for cryogenic magnetic energy and field transfer.

I would strongly recommend, based on the findings of myself, Even and van den Berg, to rebuild this flux pump with improved circuit elements. For example, the coupling factor between the primary and secondary coils is very bad. This could be achieved by positioning them on a common soft iron core. Another example would be to rebuild the inductors with superconducting wires that can withstand larger currents and avoid short circuits.

6 References

[1] T. Bernat, D. Blair and W. O. Hamilton, "Automated flux pump for energizing high curren superconductinf loads," *Rev. Sci. Instrum.,* vol. 48, no. 5, pp. 582-585, 1975.

[2] L. van de Klunder and H. ten Kate, "Fully superconducting rectifiers and fluxpumps. Part 1 1: Realized metods of pumping flux," *Cryogenics,* pp. 195-206, April 1981.

[3] W. van den Berg, "Research and Development of a Flux Pump System for Satellite Application," Saxion University/ SRON Groningen, 2015.

[4] L. Even, "Design and Characterization of a LTS Flux Pump System for Possible Satellite Application," University of Groningen/ SRON Groningen, Groningen, 2016.

[5] "Facts & Figures SRON," SRON, [Online]. Available: https://www.sron.nl/facts-figures. [Accessed 15 05 2017].

[6] P. Roelfsema, "Missions: SPICA/ SAFARI," SRON, [Online]. Available: www.sron.nl/missions-spica-safari. [Accessed 17 May 2017].

[7] M. S. Dresselhaus, "Part II - Optical Properties of Solids," in *Solid State Physics*, Massachusetts Institute of Technology.

[8] D. J. Griggiths, "7.2.3 Inductance," in *Introduction to Electrodynamics*, Pearson New International Edition, 2013, pp. 310-313.

[9] "Superconducting Magnets," Hyperphysics, [Online]. Available: http://hyperphysics.phy-astr.gsu.edu/hbase/Solids/scmag.html. [Accessed 26 June 2017].

[10] T. Peterson, "Explain it in 60 seconds: Magnet Quench," Symmetry Magazine, [Online]. Available: http://www.symmetrymagazine.org/article/november-2008/explain-it-in-60-seconds-magnet-quench. [Accessed 26 June 2017].

[11] G. Mulder, H. Krooshopp, A. Nijhuis, H. v. d. K. ten Kate and L.J.M., "A High-Power Magnetically Switched Superconducting Rectifier Operation at 5 Hz," *IEEE Transactions on Magnetics,* Vols. MAG-23, no. 2, pp. 595-598, 1987.

[12] H. H. ten Kate, P. B. Bunk, H. A. Steffens and L. J. van de Klundert, "A Thermally Switched 9 kA Superconducting Rectifier Fluxpump," *IEEE Transactions on Magnetics,* Vols. MAG-17, no. 5, pp. 2067-2070, 1981.

[13] O. Shevchenko, H. ten Kate, H. Krooshoop, N. Markovsky and Mulder.G.B.J., "Development of a 50-60 Hz Thermally Switched Superconducting Rectifier," *IEEE*

Transaction on Applied Superconductivity, vol. 3, no. 1, pp. 590-593, 1993.

[14] G. Mulder, H. ten Kate, H. Krooshoop and v. d. K. L.J.M., "Development of a Thermally Switched Superconducting Rectifier for 100 kA," *IEEE Transactions on Magnetics,* vol. 27, no. 2, pp. 2333-2336, 1991.

[15] S. Bernard and D. L. Atherton, "Performance analysis of transformer-rectifier flux pumps," *American Institute of Physics,* vol. 48, no. 10, pp. 1245-1249, 1977.

[16] "Lesson: Solenoids," Teach Engineering, [Online]. Available: https://www.teachengineering.org/lessons/view/van_mri_lesson_6. [Accessed 5 June 2017].

[17] "Hall Effect Sensor," Electronics Tutorials, [Online]. Available: http://www.electronics-tutorials.ws/electromagnetism/hall-effect.html. [Accessed 6 July 2017].

[18] "Solenoid Feild from Ampere's Law," Hyperphysics, [Online]. Available: http://hyperphysics.phy-astr.gsu.edu/hbase/magnetic/solenoid.html. [Accessed 1 July 2017].

[19] D. Atherton, "Flux pump efficency," *Cryogenics,* vol. 51, no. 7, 1967.

[20] L. Klundert, t. Kate and H.H.J., "On fully superconducting rectifiers and flux pumps. A review. Part 2: Commutation modes, characteristics and switches," *Cryogenics,* pp. 267-277, 1981.

[21] G. Pilbratt, J. Reidinger, T. Passvogel, G. Grone, D. Doyle, U. Gageur, A. Heras, C. Jewell, L. Metcalfe, S. Ott and M. Schmidt, "Herschel Space Obdervatory - An ESA facility for far-infared and submillitemeter astronony," *Astronomy & Astrophysics manuscript,* vol. (c) ESN 2010, no. Manuscript no. 14759glp, 2010.

[22] N. Morton, B. W. James, G. H. Wostenholm and R. Nichols, "The electrical resistivity of niobium and niobium-zirconium alloys," IOPscience, United Kingdom, 1975.

7 Appendices

Appendix 7.a – Wiring Pinout

Below is table which specifies the pin outs for the wiring of the cryostat, break boxes, power supplies etc.

Channel Number	Circuit Element	Type of Measurement	Connection Type	Cryostat Connector 1	Cryostat Connector 2	Break Box 1 to		Break Box 2	Break Box 3	
101	Temperature Sensor (Cernox)	Ω – 4 way	I +	'	Connected to Beak Box 1 via a DC-25 Sub cable	11	→	1	-	
			I -	'		23	→	2	-	
			V +	'		12	→	24	-	
			V -	'		24	→	25	-	
102	Extra secondary copper coil leads	Voltage – 2 way	V +	'		9	→	3	-	
			V -	'		21	→	4	-	
103	Hall Sensor	Voltage – 2 way	V +	'		3	→	5	-	
			V -	'		15	→	6	-	
104	Load coil leads	Voltage – 2 way	V +	'		6	→	7	-	
			V -	-		18	→	8	-	
105	Heater 1	Voltage – 2 way	V +	-		7	→	9	-	
			V -	-		19	→	10	-	
106	Heater 2	Voltage – 2 way	V +	-		8	→	11	-	
			V -	-		20	→	12	-	
107	Fluxgate Meter	Voltage – 2 way	V +	1 2		-		13	-	
			V -	14 15		-		14	-	
108	Primary Coil Leads	Voltage – 2 way	V +	-		13	→	15	-	
			V -	-		25	→	16	-	
121	Hall Sensor	Current – 2 way	I +	-		2	→	46	-	
			I -	-		14	→	47	-	
122	Primary Current	Current – 2 way	I +	3 to 13		-	→	48	-	
			I -	16 to 25		-	→	49	-	
221	Heater 1	Current 2 –way	I +	-		4	→		47	46 → Power Supply +25 V
			I -	-		16	→	Power Supply Com.		
222	Heater 2	Current – 2 way	I +	-		5	→		49	48 → Power Supply -25 V
			I -	-		17	→	Power Supply Com.		

Appendix 7.b – LabVIEW Script for Primary Wave

Below is the programming code used for generating the primary wave signal in LabVIEW.

```
float64 Tcom, Tup, Tdown, Ttotal, freq;
int N, Nup, Ndown, Nopen, Nclose, Ncom, N1, N2, N3, N4, N5;

// Commutation time follows from Imax and dIcom/dt
Tcom = (delta*Imax)/IdotC;
// Rise time follows from Imax and Idot
Tup = Imax/Idot;
// Fall time follows drom Imax, delta and dI/dt
Tdown = ((1-delta)*Imax)/Idot;
// Total time for 1 period of signal
Ttotal = Nperiod*(Tup+Tdown+Topen+Tclose+Tcom);
// Frequency to set in waveform generator to get the right times
freq = 1/Ttotal;

N = Ttotal*SampleRate;

// Times to discretes time
Nup = (Tup/Ttotal)*N;
Ndown = (Tdown/Ttotal)*N;
Nopen = (Topen/Ttotal)*N;
Nclose = (Tclose/Ttotal)*N;
Ncom = (Tcom/Ttotal)*N;

//Discrete time points

N1 = Nup;
N2 = Nup+Nclose;
N3 = Nup+Nclose+Ncom;
N4 = Nup+Nclose+Ncom+Nopen;
N5 = Nup+Nclose+Ncom+Nopen+Ndown;

//Generating half period of signal
int i, j, k, h;

for (i=1; i <=N/Nperiod; i++) {

        if (i <= N1) {
                I[i] = (i/N1)*Imax;

        }

if (i > N1 && i <= N2) {
        I[i] = Imax;
        }

if (i > N2 && i <= N3) {
        I[i] = Imax*(1-(delta*((i-N2)/(N3-N2))));
        }
```

```
if (i > N3 && i <= N4) {
        I[i] = Imax*(1-delta);
        }

if (i > N4 && i <= N5) {
        I[i] = (Imax*(1-delta))*(1-((i-N4)/(N5-N4)));
        }
}

//Mirroring of first half of signal to second half
if(Nperiod == 2){
        for (j=1+N/2;j <=N; j++) {
                I[j] = -(I[j-(N/2)]);
        }
}
```

Appendix 7.c – Temperature graphs for section 4.4

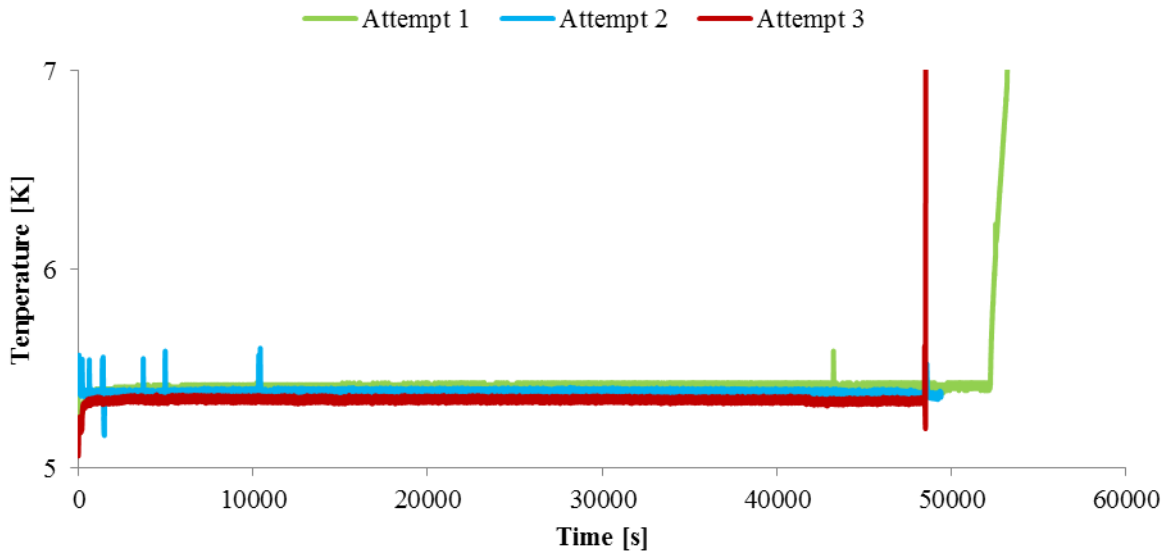

GRAPH 7.1 Shown is the temperature as detected by Cernox sensor. You can see for attempt 1 (green) and attempt 3 (red) where the liquid helium had totally evaporated. Because both attempt 2 (blue) and attempt 3 quenched at approximately the same time, the temperature spike isn't visible where "heater 1" got stuck.